Spin Dependent Transport and Magnetic Ordering in Rare Earth Metals

Infrared Spectroscopy on Holmium

Von der Fakultät für Mathematik und Physik der Universität Stuttgart
zur Erlangung der Würde eines Doktors der
Naturwissenschaften (Dr. rer. nat.) genehmigte Abhandlung

Vorgelegt von

Peter Weber

aus Neuss

Hauptberichter:	Prof. Dr. M. Dressel
Mitberichterin:	Prof. Dr. G. Schütz
Tag der mündlichen Prüfung:	14. Juli 2004

1. Physikalisches Institut der Universität Stuttgart
2004

Contents

Chapter 1

Deutschsprachige Zusammenfassung

Seit den frühen Tagen der Informationstechnologie sind magnetische Materialien aus dieser Branche nicht mehr wegzudenken. Seien es klassische Massenspeichermedien, wie Magnetband, Diskette oder Festplatte, oder schnelle magnetische Random Access Memories (MRAM): Grundlagenforschung im Bereich der Festkörperphysik ist der treibende Motor für eine ständige Verbesserung der Leistungsfähigkeit von Speichermedien. Nicht zuletzt seit der Entdeckung des "Giant Magneto-Resistance (GMR)" Effektes durch Baibich et al. and Binasch et al. [1, 2] in den Jahren 1988/89 spielen magnetische Schichtstrukturen eine wichtige Rolle in der kommerziellen Anwendung. Die Physik, die hinter diesem Effekt steckt, beruht auf der Austauschwechselwirkung zwischen dünnen magnetischen Schichten über eine nichtmagnetische, metallische Zwischenschicht hinweg [3]. Die Leitungselektronen des Metalls vermitteln indirekt eine magnetische Wechselwirkung der getrennten magnetischen Schichten. Eine solche Wechselwirkung existiert allerdings nicht nur in künstlich geschaffenen Schichtstrukturen. Einige wenige Elemente des Periodensystems arrangieren sich selber im Metallverbund in magnetischen Schichten auf der kleinstmöglichen Längenenskala: In atomaren Größenordnungen. Diese Elemente sind unter den Seltenen Erden (Lan-

thaniden) zu finden.

Die Seltenen Erden verdanken die exponierte Lage im Periodensystem der Elemente ihrer unvollständig gefüllten 4f Elektronenschale. Die 4f Elektronen sind tief im Innern der Elektronenwolke lokalisiert. Demzufolge partizipieren sie nicht an chemischen Bindungen, sind im Metallverband vom umgebenden Gitter abgeschirmt und rufen lokalisierte magnetische Momente an den Gitterplätzen hervor. Diese lokalen Momente werden durch indirekte Austauschwechselwirkung, vermittels der delokalisierten Leitungselektronen, gekoppelt, und bringen eine Vielfalt verschiedener magnetisch geordneter Strukturen hervor [49, 51]. Das allseits anerkannte Modell für diese Wechselwirkung ist die RKKY- Austauschwechselwirkung (nach: Ruderman, Kittel, Kasuya und Yosida [59, 56]).

In den letzten Jahren wurde verstärkt der Einfluss der magnetischen Ordnung in Seltenen Erden und ihren Oxiden auf die Bandstruktur untersucht. Vor allem wurden Photo-Emissionsmessungen durchgeführt [62, 64, 63, 66], um die Aufspaltung der Valenz-Bänder im Austauschfeld der sich ordnenden lokalen Momente zu erforschen. Die experimentellen Ergebnisse waren konsistent mit theoretischen Bandstrukturrechnungen [67, 68], welche eine Temperaturabhängigkeit für die Bandaufspaltung vorhersagten, je nach dem, ob die Elektronen in den untersuchten Bänder eher lokalisiert oder delokalisiert sind.

Bereits in den siebziger Jahren wurden optische Messungen an einigen Seltenen Erden vorgenommen [29, 31, 32]. Auch sie zeugten von einer temperaturabhängigen Änderung in den Spektren, die mit der oben erwähnten Bandaufspaltung in Verbindung gebracht wurde. Allerdings reichten die meisten Messungen im Frequenzbereich nicht weit genug herab, um die charakteristische Struktur vollständig zu erfassen. Außerdem wurden die Messungen nur bei sehr wenigen verschiedenen Temperaturen durchgeführt. Daher war es eine interessante Herausforderung, in dem entsprechenden spektralen Bereich temperaturabhängige Messungen durchzuführen und die Änderungen im Spektrum nachzuvollziehen. Ähnliche Messungen wurden bereits von

Knyazev und Sandratskii [Knyazev1991] durchgeführt: Sie untersuchten die Seltenen Erden Gadolinium, Terbium und Dysprosium mit der Methode der Ellipsometrie. Im Vergleich zu deren Messungen erlaubt die hier verwandte Technik der "Fourier transform infrared spectroscopy" (FTIR) eine Ausdehnung des Messbereiches um eine Größenordnung bis unter 100 cm^{-1}. In diesem Spektralbereich erwachsen weitere Fragen: Theoretische Berechnungen [72] sagen voraus, dass es aufgrund einer Hybridisierung von 4f Niveaus mit Valenzbändern [69] zu einem erheblichen Anwachsen der Zustandsdichte um die Fermi- Energie herum kommt. Dies könnte sich auch im optischen Spektrum bei kleiner Energie niederschlagen. Weiterhin ermöglicht dieser Frequenzbereich eine Überprüfung des Drude- Verhaltens der freien Elektronen [5] des Metalls.

Im Rahmen dieser Arbeit wurden die optischen Eigenschaften der Seltenen Erde Holmium untersucht. Holmium zeigt bei weitem die facettenreichsten magnetischen Strukturen vom Paramagnetismus über eine helikal antiferromagnetische Phase bis zum kegelförmig helikalen Ferromagnetismus [49, 51]. Von allen Seltenen Erden verfügt Holmium über das größte magnetische Moment pro Atom. Im Bereich von 50 cm^{-1} (6 meV) bis 10000 cm^{-1} (1 eV) wurde die Temperaturabhängigkeit, und damit die Abhängigkeit von der magnetischen Ordnung, der optischen Eigenschaften untersucht. Die gemessene Größe war die Reflektivität der Proben. Mit Hilfe des Drude-Lorentz Modells wurden die gemessenen Spektren extrapoliert, so dass durch eine Kramers-Kronig Analyse die frequenzabhängige Leitfähigkeit bestimmt werden konnte. Das Drude-Lorentz Modell erlaubte außerdem eine Separation der verschiedenen elektronischen Beiträge zu den Spektren, also des Drude-Beitrages der freien Elektronen und der verschiedenen Anregungen zwischen Bändern.

Im mittleren Infraroten wurde eine temperaturabhängige Anregung beobachtet, die mit der Aufspaltung der Valenzbänder im Austauschfeld der sich ordnenden lokalen Momente identifiziert werden konnte. Die Struktur taucht unterhalb der Néel Temperatur von 133 K auf, sättigt bei etwa 30 K

und zeigt beim Übergang in die ferromagnetische Phase unter 20 K keine erkennbare Änderung mehr. Für Holmium-Einkristalle wurden Messungen mit Licht zweier Polarisationsrichtungen durchgeführt: Zum einen parallel zur c-Achse des Kristalls und zum anderen in den Ebenen des hcp-Gitters orientiert (parallel zur a-Achse). Die qualitative Aussage, dass die magnetische Struktur in c-Polarisation wesentlich ausgeprägter ist [28], bestätigte sich. Der Unterschied im spektralen Gewicht der Anregungen der jeweiligen Polarisation beträgt etwa 25%. Im Gegensatz zu früheren optischen Messungen [28] enthüllte die detaillierte Modellierung nach Drude und Lorentz eine, wenn auch geringe, Temperaturabhängigkeit der Aufspaltungsenergie. Bei geringen Temperaturen befindet sich das Maximum der Anregung bei 3300 cm^{-1} (0.41 eV) für die a-Polarisation (in den Ebenen) und bei 3170 cm^{-1} (0.39 eV) für die c-Polarisation (senkrecht zu den Ebenen). Mit steigender Temperatur verschiebt sich das Maximum hin zu kleineren Frequenzen. Diese Beobachtungen können mit theoretischen Ergebnissen [67, 68] in Einklang gebracht werden, die eine Abhängigkeit des Temperaturverhaltens vom Grad der räumlichen Lokalisierung der Bänder vorhersagen. Es wurde vorgeschlagen, dass die beteiligten Bänder in den Ebenen des hcp-Gitters delokalisiert, senkrecht dazu aber stark lokalisiert sind [63, 64]. Diese Interpretation erklärt, dass die Aufspaltung auch in den nicht kollinear magnetisch geordneten Phasen von Holmium besteht. Die in den Ebenen delokalisierten Elektronen "sehen" dann nur die ferromagnetische Ordnung der einzelnen Ebenen. Die hier gezeigten Messungen bestätigen durch die Temperaturabhängigkeit der Austauschaufspaltung prinzipiell diese Vorstellung. Die optische Ergebnisse zeigen allerdings eine viel geringere Temperaturabhängigkeit, als die Resultate von Photo-Emissionsmessungen [63, 64]. Die optische Methode scheint, in Einklang mit Knyazev und Sandratskii [28], einen wesentlich stärker lokalisierten Bereich der Bandstruktur zu sondieren. Für die a-Polarisation ist die Anregung bereits über 120 K (also unterhalb des Phasenüberganges) nicht mehr nachzuweisen. In c-Polarisation dagegen scheint ein kleiner Beitrag sogar in der paramagnetischen Phase erhalten zu

bleiben.

Weiterhin wurden mit Holmium-Einkristallen magnetfeldabhängige optische Messungen durchgeführt. Es stellte sich heraus, dass in der antiferromagnetischen Phase mit zunehmendem externem Magnetfeld die zuvor diskutierte Struktur verschwindet. Die Änderungen im Spektrum zeigen dabei hysteretisches Verhalten. Die zentrale Frage, die sich in dieser Hinsicht stellt, ist die folgende: Warum verschwindet die Austauschaufspaltung, obwohl doch das externe Feld eine ideal parallele Ausrichtung aller magnetischen Momente bewirkt? Ein Versuch der Erklärung wäre der, dass im Magnetfeld die Fermi-Oberfläche maßgeblich deformiert wird, und dadurch eine optische Anregung nicht mehr möglich ist. Eine Deformation der Fermi-Oberfläche kann auch direkt die Austauschwechselwirkung zwischen Valenzelektronen und lokalen magnetischen Momenten beeinflussen. Auch wäre es möglich, dass das Feld die Spin-Bahn-Kopplung reduziert. Die Aufspaltung wäre dann durchaus noch vorhanden, aber der Übergang wäre optisch nicht mehr erlaubt. Beide Argumente haben einen Schwachpunkt. Bei der Wechselwirkung der paramagnetischen Bandelektronen mit einem externen Magnetfeld würde man kein hysteretisches Verhalten erwarten. Vielmehr impliziert die Hysterese eine Wechselwirkung der Bandelektronen mit den lokalen magnetischen Momenten, die wiederum durch das Magnetfeld beeinflusst werden.

Im ferninfraroten Teil des Spektrums wurden Messungen bis herab zu 50 cm^{-1} durchgeführt. Die Transporteigenschaften sind in diesem Bereich im Wesentlichen durch den Drude-Beitrag der freien Elektronen gegeben. Die gemessene Gleichstromleitfähigkeit ist konsistent mit den Reflektivitätsspektren in diesem Frequenzbereich. Aber zusätzlich sind außergewöhnliche Anregungen niederer Energie unterhalb von 400 cm^{-1} zu beobachten. Sie lassen sich in Einklang bringen mit theoretischen Berechnungen [72], die eine stark erhöhte Zustandsdichte im Bereich der Fermi-Energie vorhersagen. Diese Änderungen in der Zustandsdichte beruhen demnach auf einer Hybridisierung zwischen lokalisierten 4f- und Bandelektronen.

Optische Messungen an Schichten haben gewisse Vorzüge gegenüber Mes-

sungen an Einkristallen. Aufgedampfte Schichten liefern ohne weitere Bearbeitungsprozesse eine ideale Oberflächenqualität. Insbesondere sind Transmissionsmessungen möglich. Es wurden Holmium-Schichten unter Ultrahochvakuum (UHV)-Bedingungen hergestellt, um zu evaluieren, ob Messungen an Schichten tatsächlich Vorteile erbringen. Mit Rücksicht auf die spektroskopische Messmethode wurde Silizium als Substrat gewählt. Aufgrund der großen Eindringtiefe infraroter Strahlung in Metalle sind sowohl für Transmissionsmessungen als auch Reflexionsmessungen relativ dicke Schichten zwischen 50 nm und 100 nm sinnvoll. Die Charakterisierung der Filme erfolgte durch Röntgenbeugung, SQUID- und Widerstandsmessungen. Die Resultate zeigen, dass die Verdampfung auf kalte Substrate (Raumtemperatur) und anschließendes Ausheilen bei relativ geringen Temperaturen (>10 h; <200 °C) gute Resultate erbringt: Die Filme haben dann eine relativ große Körnung mit Kristallit-Größen um die 60 nm, und es besteht eine Vorzugsorientierung der Kristallite mit ihren hcp-Ebenen parallel zur Fläche der Schicht. Selbst nach langem Kontakt mit der Atmosphäre konnte die Oxidschicht mit einer Dicke von nur 2 nm abgeschätzt werden. Das ist nur ein Bruchteil der Eindringtiefe der Strahlung in die Schicht. Somit ist eine Wechselwirkung mit der Oxidschicht vernachlässigbar gegenüber der Wechselwirkung mit dem eigentlichen Material. Die optischen Messungen reproduzierten die Ergebnisse der Einkristall-Messungen. Die Reproduzierbarkeit der Spektren für verschiedene Filme ist gut, was bestätigt, dass die Messmethode nicht empfindlich auf Verunreinigungen auf der Oberfläche der Filme oder auf kleine Schwankungen der Herstellungsparameter reagiert. Es wurde weiterhin gezeigt, dass das Schichtsystem Holmium/Silizium mit dem Drude-Lorentz Schema modelliert werden kann, um die optischen Parameter der Holmiumschicht aus den Daten des Systemes zu extrahieren.

Im Rahmen dieser Dissertation wurden die optischen Eigenschaften von einkristallinem Holmium im infraroten Spektralbereich temperaturabhängig und magnetfeldabhängig untersucht. Techniken für Präparation, optische Messung und Datenauswertung in Hinblick auf Holmium-Schichten wurden

entwickelt. Das nächste Ziel ist es, Transmissionsmessungen an Schichten durchzuführen. So kann die Grenze des Messbereiches weiter zu kleineren Frequenzen verschoben werden. Die vorhandenen optischen Techniken erlauben Messungen bis herab zu einer Wellenzahl (0.1 meV). Die Resultate werden weiteren Aufschluss geben über das Verhalten der freien Elektronen in elementaren "Local Moment Systems", und es wird eine detailliertere Diskussion der hier beschriebenen niederenergetischen Anregungen möglich sein. Weitere Experimente sollten in Hinsicht auf das Verhalten der Austauschaufspaltung in externen Magnetfeldern durchgeführt werden. Messungen bei verschiedenen Temperaturen und höheren Magnetfeldern können bei der Beantwortung der noch offenen Fragen helfen.

Chapter 2

Introduction

Since its early days, information technology is unthinkable without magnetic materials. Let it be the classical magnetic disc, or fast magnetic random access memories (MRAM): Fundamental solid-state physics research is the driving motor for the increasing performance of storage media. Layered systems of thin magnetic films took an important part, since the discovery of the giant magneto-resistance effect (GMR) by Baibich et al. and Binasch et al. [1, 2] in 1988/89. The physics behind this effect, which was quickly utilized in commercially available hard disc read heads, is exchange coupling between nano-scale magnetic films across a nonmagnetic metal inter-layer [3]. Conduction electrons of the non-magnetic metal mediate an interaction between the separated magnetic films. But such an indirect interaction does not only occur within artificial structures. A few elements in the periodic table spontaneously self-organize in magnetic layers on the lowest possible level: On atomic scale. These elements are found among the rare earth metals (lanthanides).

The rare earth metals owe their prominent position in the periodic table of elements to their unfilled 4f electron shells. As these shells are localized within the atomic ion core, they do not participate in any bonding, and thus, give rise to localized magnetic moments in the metallic state. These local moments may get exchange-coupled via delocalized conduction electrons

and exhibit a wide variety of magnetically ordered structures [49, 51]. The well accepted model for the exchange mechanism is RKKY exchange (after: Ruderman, Kittel, Kasuya, and Yosida [59, 56]), being just recently enforced by spin-polarization experiments of Hindmarch and Hickey [57].

In the last years, the focus was increasingly put on the influence of magnetic ordering in rare earth metals and oxides on their band structure and vice versa. Especially photo-emission measurements were carried out [66, 62, 65, 64], to explore the band splitting of valence bands in the exchange field of the localized, ordered magnetic moments. The experiments were in accordance with theories [67, 68], which predicted the temperature dependence of the splitting being influenced by the degree of delocalization of the particular bands.

Already in the seventies, optical infrared measurements were carried out on several rare earth metals, which indicated the existence of a magnetic splitting feature [29, 32, 31]. But most of the spectra did not reach far enough to low frequencies, and thus, only touched the rising edge of the feature. Additionally, those measurements were carried out only at a few different temperatures. Thus, it was a challenging task, to carry out optical measurements in the corresponding frequency range, and shine some light on the temperature dependence of this optically observed magnetic feature. Similar measurements were carried out by Knyazev and Sandratskii [28] on gadolinium, terbium, and dysprosium, using ellipsometry. Our technique of Fourier transform infrared spectroscopy (FTIR) allows to extend the frequency range by an order of magnitude (below 100 cm^{-1}). In this spectral region, additional questions arise: Theoretical calculations predict, that, due to a hybridization of 4-f electrons with valence bands [69], there occurs an unusually high density of states in closest vicinity to the Fermi level [72]. This might also be reflected in the low-energy optical spectra. Furthermore, the low-frequency part of the spectra yields a picture of the free electrons' behaviour [5].

The rare earth metal of choice was holmium. It shows the widest vari-

ety of magnetic states of all rare earth metals. In contrast to gadolinium, terbium, and dysprosium (examined in [28]), it also features a non-collinear, ferromagnetic state. Of special interest is the effect of an external magnetic field on the spectra, enforcing an all-parallel orientation of the magnetic moments (like in gadolinium, terbium, or dysprosium). Measurements were carried out on bulk single crystals, as well as on films.

After this brief introduction, the third chapter will deal with rare earth magnetism. The remarkable properties of the lanthanides are compared with the transition metals. The importance of the localized 4-f electron shells is pointed out, and the indirect exchange interaction between the local moments is described. Finally, the magnetic structure and the properties of holmium are specified. In chapter four, electron-transport properties of metals are discussed. The Drude and the Lorentz model are used, to give a picture of dc resistivity as well as optical conductivity. The temperature-dependent dc resistivity of holmium is given, and an overview is supplied on its optical properties, as far as already explored. The fifth chapter describes the preparation and characterization of holmium films. The choice of substrate, as well as interface effects are discussed. The used ultra-high vacuum (UHV) chamber and the process of evaporation are described. Results of X-ray diffraction, SQUID, and resistivity measurements on the films are presented. In the sixth chapter, finally the results of the optical measurements are presented. In a brief section, the Fourier transform infrared spectrometer is described. Reflection spectra are shown, and the process of extrapolation and calculation of the frequency-dependent conductivity is explained. By the help of Drude-Lorentz fits, different electronic contributions to the spectra are extracted and discussed. Special care is taken on the temperature-dependent changes in the spectra due to magnetic phase transitions. The results of the field-dependent measurements are presented. Spectra of bulk single crystals and different films are compared. The last chapter summarizes the results and conclusions of the project.

Chapter 3

Rare earth Magnetism

A most amazing effect arises, when several electrons are put together and are treated as one many-particle system. By virtue of their Fermionic character, an additional interaction occurs: Exchange! This interaction is a consequence of the fact, that two identical particles cannot be distinguished in quantum physics [39]. For a system of electrons, out of the set of solutions of Schrödinger's equation, only the antisymmetric ones (in terms of particle exchange) are allowed states. Those states can be expressed by the Slater determinant. The heuristic formulation of the Pauli exclusion principle, then follows easily from the general properties of the determinant [40]. Exchange interaction between electrons, on the other hand, is a straightforward consequence of the exclusion principle: The probability density in space depends on the relative orientation of the spins, and different spatial wave functions correspond to different energy eigenvalues, due to coulomb repulsion. In the shape of Hund's rules, the Pauli principle governs the electronic and magnetic structure within the atom(see table 3.1). In solid state it is responsible for band structure and magnetic ordering.

Magnetic properties of the rare earth metals differ, in many aspects, from those of other metals in the periodic table of elements. To point out the prominent part of rare earths among the magnetic metals, the first section of the chapter gives a brief overview on the general magnetic properties of

metals. The second section deals with electronic structure of the rare earth 3+ ion cores and indirect exchange between their localized magnetic moments in the metal. Finally, the magnetic structure of holmium is described.

3.1 Magnetic Moments in Metals

This section shall give a short overview on the magnetic properties of metals, to distinguish the outstanding position of the rare earths. The metallic elements feature a wide variety of magnetic effects. Leaving magnetic ordering aside, there may be four possible contributions to magnetic susceptibility in a metal: Ion cores contribute, depending on their electronic structure, with diamagnetic and, in some cases, with paramagnetic moments. Conduction electrons always contribute with both [43].

In a rough classification, metals can either have closed or open ion-core electron shells. Those with open core-shells can be further subdivided into transition metals with open d shells, and lanthanides and actinides respectively having open f shells.

In this strict definition, the lanthanides and actinides would only range from cerium (i.e. thorium) to thulium (i.e. mendelevium). Lanthanum, yterbium and lutetium as well as actinium, nobelium Lawrencium have filled shells. Nevertheless, in Mendelejev's periodic table they are accounted for the lanthanides and actinides due to their very similar chemical properties. With respect to magnetism, they differ dramatically.

The fraction of transition metals includes the elements between third and tenth period. Copper, silver and gold have closed d shells, and thus do not belong to the transition metals according to their magnetic properties. They also owe their prominent position only to their valence-electron configuration.

Generally those metals positioned to the left of the transition metals have positive magnetic susceptibilities, while those to the right have negative ones. The only exception is aluminium, having a positive susceptibility. All these metals have in common, that their ion cores consist of closed shells. Thus

the cores do not contribute with a paramagnetic, but only with a diamagnetic moment. Van Vleck paramagnetism (induced paramagnetic moment of the core electrons due to coupling of the different multiplet states) as well as paramagnetic contribution of the conduction electrons is usually small. Only for the alkali metals, the alkali-earth metals and for aluminium it is larger than the diamagnetic contributions of core and conduction electrons. All metals in between, i.e. those with open inner shells, have relatively large positive susceptibilities, when compared to the previously mentioned ones. This is due to the fact, that the open inner shells result in a total paramagnetic moment for each ion core, while for closed shells, the magnetic moment cancels out.

Before the magnetic properties of rare earth metals are discussed, the crucial difference to the transition metals shall be pointed out. Both species possess open inner shells, 4f shells in the case of rare earths, and 3d, 4d or 5d shells respectively in the case of transition metals. The latter are rather delocalized. Their wave functions reach far enough, to overlap with the respective neighbouring wave functions. The term inner shell is somewhat misleading in the case of the transition metals. Magnetic ordering in such d-systems is contributed to exchange interaction between the spins of these overlapping shells. In contrast to the state of affairs within transition metals, the 4f electrons of rare earth ion cores are almost fully localized. Surrounded by the filled 5s and 5p shells they are well screened from the surrounding lattice (see figure 3.1). The crystal field splitting is negligible against the separation of the spin-multiplet states. For the 4f levels there is no overlap with the neighbourhood, and the states of the free atom remain largely intact. Exchange interaction between the localized spins of 4f shells is an indirect one, being mediated by the 6s and, if available, the 5d conduction electrons (see section 3.2.2).

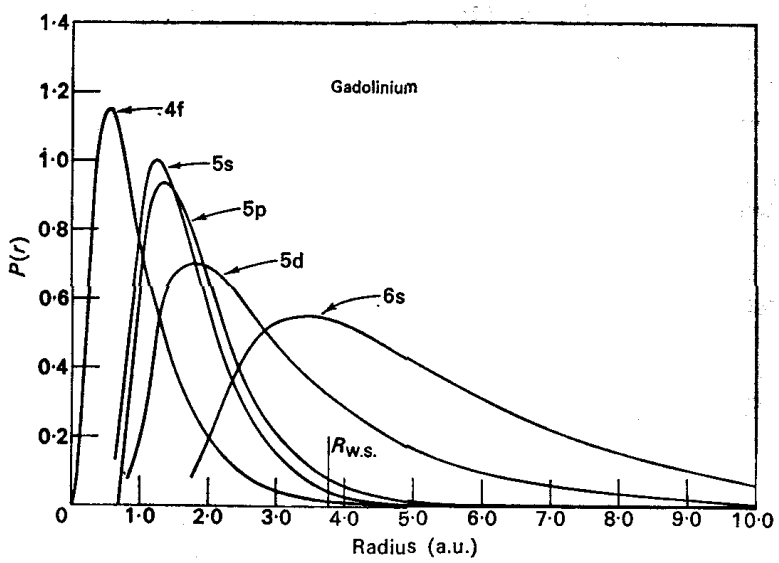

Figure 3.1: Radial distribution of the electronic wave functions in gadolinium [47]. The open 4f shells are screened by the closed 5s and 5p shells. $R_{W.S.}$ is the half inter-ionic distance in the metal. Thus there is a wide overlap between the neighbouring 5d and 6s wave functions.

3.2 Magnetism in Rare Earth Metals

The rare earth metals feature a rich variety of magnetic ordering schemes. They owe their prominent position among the magnetic elements to their localized magnetic moments, which interact indirectly via conduction bands. Within their period, the magnetic moments of the rare earth atoms are tuned with increasing atomic number. The interplay of local magnetic moments, spatial electron distribution and periodic exchange coupling nurtures exotic magnetic structures, culminating in the cone-helical ordering of holmium. As exchange interaction is strongly influenced by the shape of the Fermi surface, those extraordinary magnetic properties are also reflected in the electron transport properties. While dc-conduction measurements were carried out exhaustively, optical experiments are rarely reported. Especially the infrared and far-infrared spectral range is supposed to reflect magnetic excitations.

$4f^n$	3+Ion	L	S	J	g	$g\sqrt{J(J+1)}$	$\mu_{para}^{exp}(\mu_B)$
0	La	0	0	0			
1	Ce	3	$\frac{1}{2}$	$\frac{5}{2}$	$\frac{6}{7}$	2.54	2.51
2	Pr	5	1	4	$\frac{4}{5}$	3.58	2.56
3	Nd	6	$\frac{3}{2}$	$\frac{9}{2}$	$\frac{8}{11}$	3.62	3.4
4	Pm	6	2	4	$\frac{3}{5}$	2.68	
5	Sm	5	$\frac{5}{2}$	$\frac{5}{2}$	$\frac{2}{7}$	0.85	1.74
6	Eu	3	3	0			
7	Gd	0	$\frac{7}{2}$	$\frac{7}{2}$	2	7.94	7.98
8	Tb	3	3	6	$\frac{3}{2}$	9.72	9.77
9	Dy	5	$\frac{5}{2}$	$\frac{15}{2}$	$\frac{4}{3}$	10.65	10.83
10	Ho	6	2	8	$\frac{5}{4}$	10.61	11.02
11	Er	6	$\frac{3}{2}$	$\frac{15}{2}$	$\frac{6}{5}$	9.85	9.9
12	Tm	5	1	6	$\frac{7}{6}$	7.56	7.61
13	Yb	3	$\frac{1}{2}$	$\frac{7}{2}$	$\frac{8}{7}$		
14	Lu	0	0	0			

Table 3.1: Quantum numbers and Landé factors for the rare earth 3+ ions. The experimental data for the paramagnetic magnetization per atom in units of μ_B for the heavy rare earths coincide well with the theoretical values [49].

Optics is the means to indirectly probe the exchange interaction between the localized magnetic moments via exchange-mediating conduction electrons.

3.2.1 3+ Ion Cores

In the metallic state rare earths use to occur as trivalent ion cores, each of the atoms contributing with three electrons to the metallic bonding. One of the inner 4f electrons is promoted to a band state and participates in the metallic bonding, together with the two 6s (and the 5d, if present) electrons. Exceptions are cerium (Ce^{4+}), europium (Eu^{2+}) and ytterbium (Yb^{2+}). They step out of the line, as a completely empty or a completely filled 4f shell is

energetically most favourable (Hund's Rules).

For magnetism the closed inner shells are of no importance, as their net magnetic moments cancel out. Valence electrons only account for a small fraction of magnetic susceptibility, although they are the essential mediators of exchange in the ordered states. Thus, the 4f electron shells are protagonists in terms of the magnetic moment. Their occupation with increasing atomic number within the period of the rare earth elements perfectly displays the validity of the Pauli principle and Hund's rules. The total angular momentum of the 4f electrons can be determined according to Russel-Saunders coupling. All orbital angular momenta $\vec{l_i}$ of all electrons are coupled via Coulomb interaction to a total orbital momentum $\vec{L}$, while all spins $\vec{s_i}$ are separately coupled by exchange interaction to the total spin momentum $\vec{S}$. For the total angular momentum $\vec{J} = \vec{L} + \vec{S}$ spin orbit coupling has to be taken into account. The degeneracy of the different possible J multiplets is lifted. In the case of a less than half-filled shell the multiplet with the lowest quantum number J has the lowest energy (i.e. $J = L - S$). For more than half-filled shells it is the other way around (i.e. $J = L + S$) [42]. Table 3.1 shows the respective quantum numbers for the rare earth metal series. The Landé factor in the case of Russel-Saunders coupling is [49]:

$$g = \frac{3}{2} + \frac{S(S+1) - L(L+1)}{2J(J+1)}. \tag{3.1}$$

The energetic distance of the lowest lying multiplet to the next higher one is large. At room temperature only the ground state is occupied . Thus the contribution of Van Vleck paramagnetism to the total paramagnetic moment, i.e. the admixture of the ground state multiplet with higher ones, is negligible (exceptions: samarium and europium [46]). When the total angular momentum of the shell is known, the paramagnetic moment of the ion can be calculated to $\vec{\mu} = g\mu_B\vec{J}$, i.e. $|\mu| = g\mu_B\sqrt{J(J+1)}$. In the case of heavy rare earth metals, the theoretically predicted values are only slightly lower than the measured ones. This is due to a contribution of the conduction elec-

trons. For high temperatures, i.e. in the paramagnetic regime, the magnetic susceptibility of rare earth metals can be well estimated by a Curie-Weiss law [45]:

$$\chi = \frac{N\mu_B^2 g^2 J(J+1)}{3k_B(T-\theta)}. \tag{3.2}$$

Here, N is the number of atoms, μ_B is the Bohr magneton, k_B is the Boltzmann factor, T is the temperature, and θ is the Curie temperature.

3.2.2 Magnetic Interaction

Previous sections dealt with the magnetic properties of rare earth 3+ ions. Their magnetic moments are the vital prerequisite for rare earth magnetism. The importance of exchange interaction for the ordering of spin magnetic moments also was pointed out. In contrast to the transition metals there is no overlap of the magnetic 4f states between neighbours. Nevertheless ordering occurs. In rare earth magnetism the conduction electrons play a chief part in mediating exchange interaction between the magnetic ion sites.

Rare Earth Band Electrons

The 5d and 6s electron states of the rare earth metals have a considerably higher energy, than the 4f states (ΔE approximately 10 eV). The latter lie within the ion core, well screened by the closed 5s and 5f shells. Figure 3.1 shows the position probability of the respective states in the case of gadolinium. The marked atomic radius implies a wide overlap for the outer shells, which results in the formation of a broad s-d conduction band. As already noted, for the heavy rare earth metals it was assumed, that one of the 4f electrons is promoted into a d state. This assumption is justified by a multitude of experimental results from crystal-structure, melting-point or heat-of-sublimation measurements. Early band structure calculations [47] do not account for any influence of 4f states on conduction bands. More

recent publications [69] include the 4f states in the band structure, and model the splitting of the 4f states into fractions of localized and band electrons. They allow ab initio calculation of the contribution of 4f levels to valency. The results predict a hybridization between 4f and 6s levels. This can lead to extraordinary high densities of states just above the Fermi level. This increased density of states was confirmed by the far-infrared measurements, presented in this work.

RKKY Interaction

Indirect (RKKY) exchange in rare earth metals acts in two steps. A localized spin magnetic moment polarizes the surrounding conduction electron spins and they, in turn, polarize the next-neighbour local spin moments. Exchange interaction between the 4f and the band electrons (s-f or s-d interaction, [52], [56], [58]) is promoted by the large overlap of the respective wave functions, and plays a fundamental part also in other physical problems like the Kondo effect. Ruderman and Kittel [59] first developed the idea of indirect exchange interaction for the coupling of nuclear magnetic moments in metals. Kasuya and Yosida applied their considerations on rare earth and transition metal systems (see also [61], [60]).

The hamiltonian for exchange between the localized spin moment $\vec{S}$ of a 4f shell and a conduction electron spin $\vec{s}$ is $I(\vec{s}\cdot\vec{S})$ with the exchange operator I. In the case of rare earth metals there exists a strong coupling between total spin $\vec{S}$ and total orbital angular momentum $\vec{L}$. Since the exchange energy is usually much smaller than the spin-orbit splitting, according to De Gennes the projection of the spin on to the total moment $(g-1)\vec{J}$ has to be taken into account. In the semi-classical picture of the spin precessing about the total magnetic moment $\vec{J}$, this can roughly be interpreted as the time average total spin of the 4f shell. Thus the Hamiltonian will take the form $I(g-1)(\vec{s}\cdot\vec{J})$. The RKKY interaction considers two of these processes: The interaction of one site-spin at the position $\vec{R}_l$ with band electrons and the interaction of an other site-spin at the position $\vec{R}_{l'}$ with the band electrons.

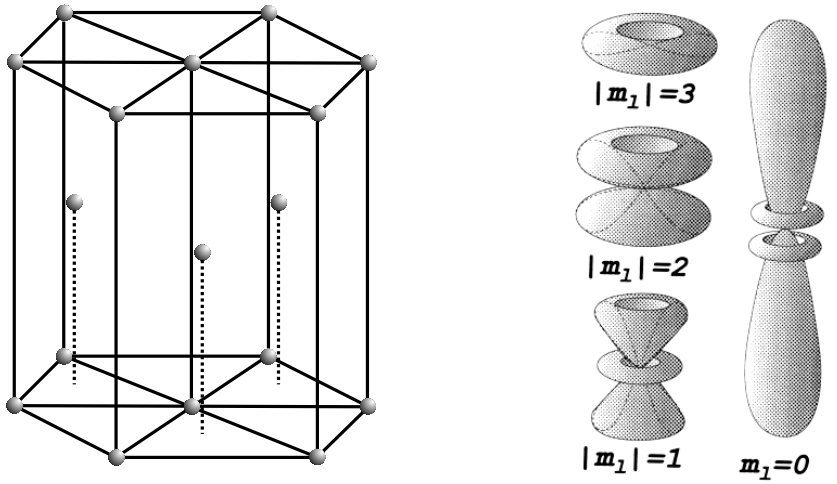

Figure 3.2: Hexagonal close packed crystal structure of holmium and the anisotropic charge cloud of the 4f electron niveaus [53].

Summation over all sites yields as expression for the RKKY-exchange hamiltonian:

$$H_{ff'} = -(g-1)^2 \sum_{l,l'} j(\vec{R}_l - \vec{R}_{l'}) \vec{J}_l \vec{J}_{l'}, \tag{3.3}$$

$$j(\vec{R}_l - \vec{R}_{l'}) = \frac{1}{N} \sum_{k,k'} |j_{sf}(\vec{k} - \vec{k}')|^2 \frac{f_k(1-f_{k'})}{E_{k'} - E_k} e^{i(\vec{k}-\vec{k}')\cdot(\vec{R}_l - \vec{R}_{l'})}. \tag{3.4}$$

Here $\vec{k}$ are the wave vectors of the conduction electrons and E_k their respective energies. f_k is the Fermi occupation function, and N is the spatial density of magnetic lattice sites. The exchange integral j_{sf} is that of the s-f interaction between local spins and conduction electrons [47, 49].

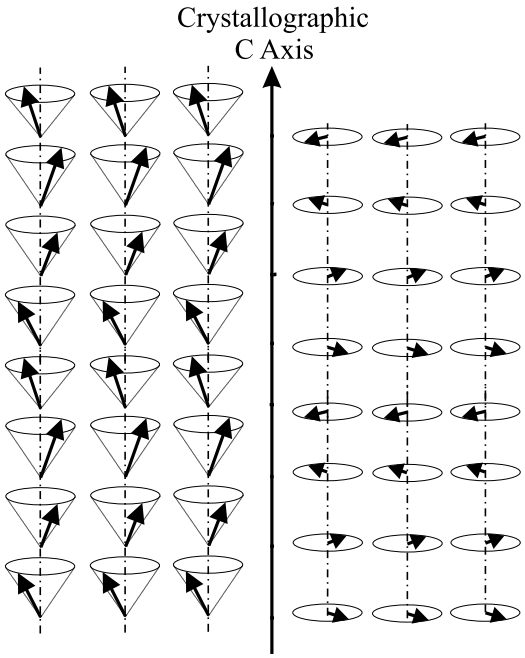

Figure 3.3: Below 133 K holmium orders in a basal-plane antiferromagnetic helical structure (right). The ferro-cone helix structure shapes below 20 K (left).

3.3 Magnetic Structure of Holmium

All heavy rare earth metals form a hexagonal close packed (hcp) lattice (3.2). They show an amazing variety of magnetic structures. The interplay of oscillating, indirect exchange and sstructured Fermi surface leads to a strongly anisotropic magnetic interaction. Figure 3.2 shows the 4f-electron charge clouds in a free ion. They constitute a pronounced electric multipole. The electrostatic crystal field of hexagonal symmetry alters these polar orbitals and, via spin-orbit coupling, strongly promotes exchange anisotropy. Oscillations of RKKY exchange interaction with ionic distance allows for ferromagnetic, as well as antiferromagnetic ordering. The rare earth metal holmium is paramagnetic above its Néel temperature of 133 K. Below, an antiferromagnetic ordering is established. Short range ordering occurs al-

ready above the Néel temperature as for example transport measurements (heat and electric conduction) reveal. The antiferromagnetic spin structure is a basal plane helix. As shown in figure 3.3, all spins are aligned within each basal plane. When propagating towards c-axis direction (perpendicular to the basal planes), the collective spin direction is turned from plane to plane for a certain angle. Just below Néel temperature this turning angle is about 50° and it decreases to about 30° at 4.2 K. The helical structure tends to be commensurable with the lattice. At 4.2 K it has a periodicity of 12 planes. At 20 K there occurs a second-order phase transition to ferromagnetic ordering. The basal plane arrangement stays the same but all moments are tilted out of the plane to form a ferro-cone helix. The opening angle of the cones is about 80° (see figure 3.3). The out-of-plane component of the magnetic moment per atom at 4.2 K is 1.7 μ_B while the in-plane component takes a value of 9.5 μ_B. Easy axis is the in-plane b-direction $(10\bar{1}0)$. Application of a field yields a saturation magnetization in that direction of 10.34 μ_B [54], [50]. It is slightly larger, than the value expected from the ionic moment ($gJ = 10$). Application of a field in-plane but deviating from b-axis direction only enforces an alignment along the latter at high enough fields. Thus the measured saturation magnetization is reduced then. The c-axis is the hard axis of magnetization. Figure 3.4 shows magnetization measurements of Strandburg, Legvold, and Spedding. The magnetic field direction was (1000), $(0\bar{1}10)$, and (0001).

In rare earth metals, conduction electrons play the crucial part in magnetic ordering. The structure of the localized magnetic moments was extensively studied by neutron scattering experiments [50]. The "deep-in" band structure was explored by photoemission [64]. But the electron structure at the very surface of the Fermi sphere, where transport takes place, can be best examined by infrared and far-infrared spectroscopy.

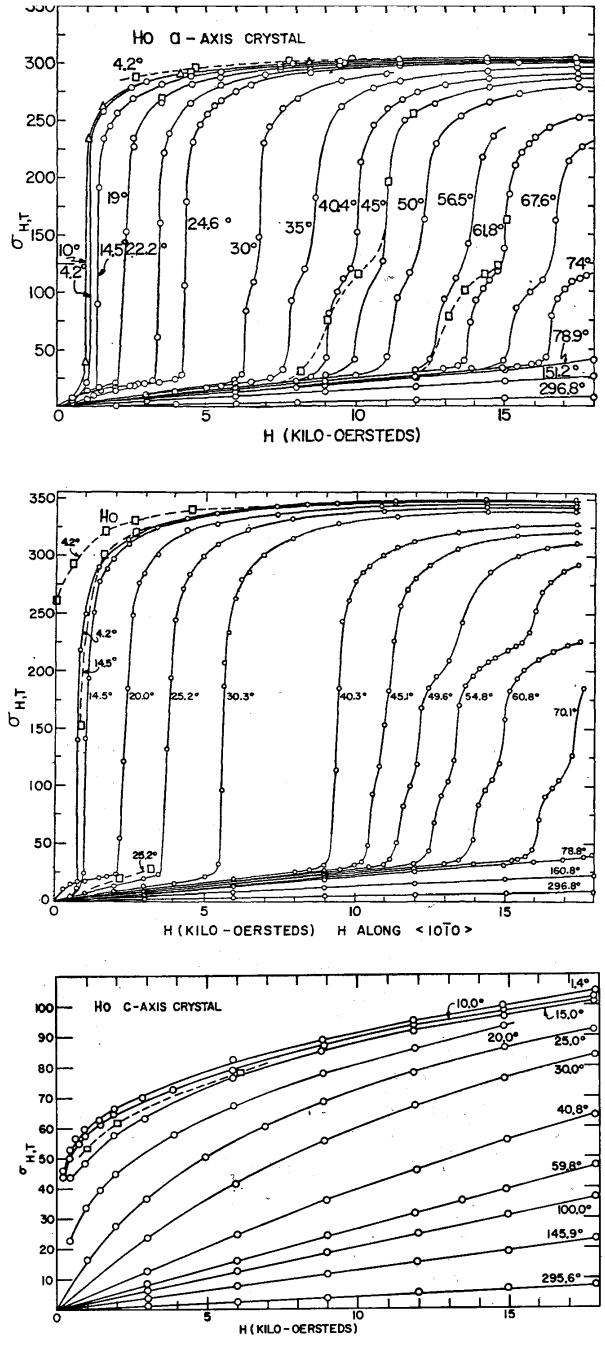

Figure 3.4: Magnetization of holmium in the three directions of the hcp crystal lattice at different temperatures [54]. From top to bottom: (1000), (0$\bar{1}$10), and (0001)

.

Chapter 4

Electron Transport in Metals

A metal can be regarded as a periodic array of positive ions, embedded in a gas of delocalized, mobile electrons. This point of view was first taken up in 1900 by Drude ([33], [34]). After quantum mechanics was established, the description of Drude was modified by Sommerfeld and is, since then, well capable of modelling electron transport properties in metals, like dc-electric conduction, heat conduction, or heat capacity [44]. The Drude-Sommerfeld model is also suitable to describe optical properties of metals. It has to be combined with the model of Lorenzian oscillators to make allowance for the fact, that part of the valence electrons are confined to filled bands. Both pictures, the Drude model as well as the Lorentz model, are rather crude ones, contradicting modern quantum theory in many aspects. But still, their combination provides a vital tool to interpret optical spectra of metals.

4.1 The Drude Sommerfeld Model

The Drude-Sommerfeld model is a simple but powerful means to describe the behaviour of conduction electrons in a metal. In allusion to charge transport in an electrolyte, Drude described electrons in a metal as randomly moving gas-like ensemble of particles. They should behave according to kinetic gas theory, the only interaction to be elastic scattering. As a consistent quan-

Element	$V_0[10^{-3}nm^3]$	Valency	$n[nm^{-3}]$	$v_F[cm/s]$	$E_F[eV]$
Li	21.62	1	47.0	1.29	4.74
Cu	11.81	1	84.7	1.57	7.00
Al	16.49	3	181	2.03	11.7
Gd	19.08	3	157	1.93	10.62
Tb	18.51	3	162	1.95	10.83
Dy	18.21	3	165	1.96	10.95
Ho	17.97	3	167	1.98	11.05
Er	17.68	3	170	1.98	11.17
Tm	17.37	3	173	1.99	11.30

Table 4.1: Fermi energies and velocities of heavy rare earth metals, calculated from the unit cell volume V_0 per atom. For calculation of the electron density n three conduction electrons per atom were assumed. The data for lithium, copper and aluminium were taken from [44].

tum theory was not yet established at that time, Drude assumed a Boltzman distribution for the electron velocity. Some time later Sommerfeld picked up Drude's considerations. He applied the concept of the Fermi sphere on Drude's findings. Table 4.1 shows Fermi energies for the magnetic heavy rare earths and for some typical metals, calculated from the free electron model [35].

4.1.1 Dc Conduction

The occupied states of a free electron gas can be described by the Fermi sphere in momentum space. In ground state (no applied field) the average momentum of all electrons is zero. The centre of the Fermi sphere is located at the origin of k-space. On applying a field, the Fermi sphere is translated from this position until acceleration and scattering of the electrons come to an equilibrium. The electrons move with average constant velocity, a current

flows along the field. As soon as the field is turned off, the Fermi sphere relaxes back to the ground state and the average velocity of all electrons vanishes (the centre of the Fermi sphere being zero momentum again). The time evolution of this process can be described by a relaxation time τ, which is an electron's average time of travel between two collisions. The equation of motion for the average electron momentum in a field E is:

$$\frac{d}{dt}\langle\vec{p}\rangle = -\frac{\langle\vec{p}\rangle}{\tau} - e\vec{E}. \tag{4.1}$$

The current density is

$$\vec{J} = -\frac{ne}{m}\vec{p} \tag{4.2}$$

with the electron (volume) density n and the electron mass m. The current density is the linear response to the externally applied stimulus, the electric field $\vec{E}$. The corresponding response function is the conductivity. In the case of a static (i.e. dc) field the change in momentum (equation 4.1) vanishes, as soon as equilibrium is established. This leads to the following expression for the dc conductivity:

$$\sigma_{dc} = \frac{J}{E} = \frac{ne^2\tau}{m}. \tag{4.3}$$

Drude's picture of gas-like electron scattering has to be regarded as a phenomenological model. Its advantage is its universality. Drude's scattering mechanism, represented by the scattering time τ, can be easily interpreted in terms of just any kind of scattering: Phonon scattering, dislocation or impurity scattering, magnetic scattering and so on. From the scattering time, the free path of a conduction electron can be calculated ($l = v_F\tau$), as the contributing electrons originate from the Fermi surface.

Element	$\rho_a[\mu\Omega cm]$	$\sigma_a[10^3(\Omega cm)^{-1}]$	$l_a[\mathring{A}]$
Li	8.55	117	17
Cu	1.65	606	5.5
Al	2.45	408	6.9
Gd	140	7.14	3.1
Tb	123	8.13	3.5
Dy	112	8.93	3.8
Ho	102	9.8	4.1
Er	58	17.2	7.1
Tm	57	17.5	7.2

Table 4.2: Measured resistivity and conductivity in plane of the hcp-structure layers. The free path was calculated from these values according to the free electron model. The data for lithium, copper and aluminium were taken from [44].

The Fermi velocities of the magnetic heavy rare earth metals, according to the free electron model, are listed in table 4.1, together with some typical metals. Table 4.2 shows scattering times and the corresponding free path lengths of the respective elements. They were calculated from measured resistivities at room temperature. The resistivity of rare earth metals is relatively high, compared to other metals. On the first view this might be puzzling, as, according to the free electron model, rare earth metals have a high electron density. But on the other hand, the model predicts a very short free path length. In other words, the model anticipates a scattering process, uncommon among most other metals. Temperature dependent measurements of rare earth's resistivity show, that, indeed, there exists an additional scattering process: Magnetic scattering. Thus, the simple free electron model with its anonymous scattering process describes qualitatively well the magnetic behaviour of the rare earth metals.

4.1.2 Ac Conduction

In the previous section electrons were supposed to move within a constant homogenous electric field. Now the response of the free electron gas to a periodic field shall be examined. As a consequence, in equation 4.1 the time derivative of the electron's spatial average momentum no longer vanishes. A periodic ansatz for electric field and electron momentum leads to the complex, frequency dependent conductivity

$$\hat{\sigma}(\omega) = \frac{ne^2\tau}{m}\frac{1}{1-i\omega\tau}. \tag{4.4}$$

The real part $\sigma_1(\omega)$ describes absorbtion (dissipation), while the imaginary part $\sigma_2(\omega)$ deals with phase change (dispersion):

$$\sigma_1(\omega) = \frac{\omega_p^2\tau}{4\pi}\frac{1}{1+\omega^2\tau^2} \qquad \sigma_2(\omega) = \frac{\omega_p^2\tau}{4\pi}\frac{\omega\tau}{1+\omega^2\tau^2}. \tag{4.5}$$

The plasma frequency ω_p is defined as

$$\omega_p = \left(\frac{4\pi ne^2}{m}\right)^{\frac{1}{2}}. \tag{4.6}$$

The zero-frequency limit of equation 4.4 links the two parameters ω_p and τ to the dc-conductivity:

$$\sigma_1(\omega = 0) = \sigma_{dc} = \frac{1}{4\pi}\omega_p^2\tau. \tag{4.7}$$

An equivalent description of a medium's response to an ac-electric field can be achieved in terms of the complex dielectric constant $\hat{\epsilon}(\omega)$ with the real and imaginary parts

$$\epsilon_1(\omega) = 1 - \frac{4\pi}{\omega}\sigma_2(\omega) \qquad \epsilon_2(\omega) = \frac{4\pi}{\omega}\sigma_1(\omega). \tag{4.8}$$

Usually $\sigma_1(\omega)$ and $\epsilon_1(\omega)$ are given, to characterize the optical properties of a medium.

Drude himself already stated, that for optical considerations parts of the valence electrons have to be assumed localized [34]. The following section will deal with electronic transitions between localized states, i.e inter-band transitions, in contrast to the continuous in-band excitations, that the completely free electrons experience. It turns out, that a mixture of free and weakly bound electrons generally describes a metal very well.

4.2 Lorentz Model and Ac Conduction

The free electron model by its own is not sufficient to describe a metal's ac conductivity (especially at higher frequencies). In addition to free electrons, weakly bound electrons have to be accounted for. The latter can only change their momentum by discrete excitation to an energetically higher, empty band above the Fermi energy. Such transitions, and their influence on optical properties, are well described by the Lorentz model [5]. It assumes the electrons in completely filled bands to behave like harmonic oscillators, which are excited by the alternating electric field. This model does not the least account for any modern theory. The picture is rather far away from an electron's behaviour in a filled band according to quantum mechanics. Thus, it is somewhat surprising, that the calculations according to the Lorentz model are in very good accordance with experimental results. Shape as well as position of absorption features in the spectra are described properly. Calculated positions suit well with corresponding band gaps, across which excitations take place. Altogether, the Lorentz model is well capable of relating optical features of a medium to its band structure.

The Lorentz model assumes a harmonic oscillator for each electron:

$$\frac{d^2\vec{r}}{dt^2} + \frac{1}{\tau}\frac{d\vec{r}}{dt} + \omega_0^2\vec{r} = -\frac{e}{m}\vec{E}(t). \tag{4.9}$$

The only difference to equation 4.1 for the free electron model is the linear term in $\vec{r}$, according to the restoring force of the oscillator. Using a periodic ansatz, i.e. assuming a time dependence with exp(-i ω t), equation 4.9 leads to the complex dielectric constant with real and imaginary part being

$$\hat{\epsilon}_1(\omega) = 1 + \frac{\omega_p^2(\omega_0^2 - \omega^2)}{(\omega_0^2 - \omega^2)^2 + \omega^2/\tau^2}, \qquad \hat{\epsilon}_2(\omega) = \frac{\omega_p^2\omega/\tau}{(\omega_0^2 - \omega^2)^2 + \omega^2/\tau^2}. \quad (4.10)$$

Real and imaginary part of the complex conductivity are:

$$\hat{\sigma}_1(\omega) = \frac{\omega_p^2}{4\pi}\frac{\omega^2/\tau}{(\omega_0^2 - \omega^2)^2 + \omega^2/\tau^2}, \qquad \hat{\sigma}_2(\omega) = -\frac{\omega_p^2}{4\pi}\frac{\omega(\omega_0^2 - \omega^2)}{(\omega_0^2 - \omega^2)^2 + \omega^2/\tau^2}. \quad (4.11)$$

The plasma frequency ω_0 of an oscillator is defined in the same way, as it was for the Drude model in equation 4.6. It denotes the "strength" of the oscillator, being proportional to the area under the peak in the conduction curve. The scattering time τ is a measure for the damping of the oscillator, being inversely proportional to the full width at half maximum of the conductivity peak. The position of the peak, i.e. its resonance frequency is ω_0. As stated in the beginning, the picture of the oscillating electron does not conform to an electron's dynamics within a band. Nevertheless, the Lorentz model fits to the data very well. The resonance frequency ω_0 has to be identified with the width of a band gap, across which an excitation takes place. The scattering time τ represents not a damping but is the time period, for which an average excited electron dwells in the upper band. The area beneath the conductivity curve of an excitation is a measure for the density of electrons, participating in the transition(according to sum rules [5, 26]).

4.3 Relevance of the Drude-Lorentz Model

The linear superposition of Drude and Lorentz model is a very powerful tool to interpret optical data. It has proven to be of high value for simple metals (gold, aluminium, etc.) [5, 24]. Results are in good accordance with theory and other, non-optical experiments like dc conductivity, specific heat or heat conduction experiments. For more complex metals, i.e. metals with a sophisticated band structure, in principle the model still holds. It may become more and more challenging, to fit all the features, that appear in the spectra. Difficulties arise mainly due to the fact, that in the case of many broad oscillators (as in metals) more and more fit parameters have to be introduced to the model, and it might loose its physical meaning. Additionally, uncertainty is drastically increased [25] with large numbers of parameters. Despite the complicated band-structure of rare earth metals, the spectra discussed in this work can be easily modelled with a few features. That makes the Drude-Lorentz model well applicable.

4.4 Electron Transport in Rare Earth Metals

The extraordinary magnetic properties of rare earth metals also have an impact on electrical conductivity. The common linear temperature dependence in dc-conductivity is altered. A typical feature for all rare earth metals is the kink at the onset of magnetic ordering. At low energies, spin waves are excited. The high scattering rate, partly due to magnetic disorder scattering, is reflected in the ac-conductivity spectra of the materials. In the magnetically ordered phase, a transition occurs, that is interpreted in terms of an exchange splitting of valence bands.

4.4.1 Dc Conduction

For "ordinary" materials, the total resistivity results from electron scattering on vacancies, dislocations, impurities, grain boundaries (residual resistivity

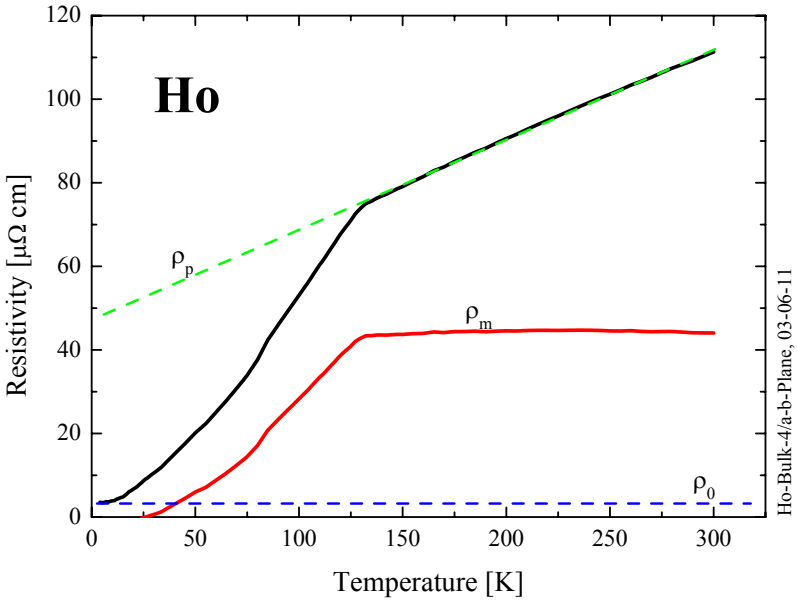

Figure 4.1: The total resistivity of a magnetic material is the sum of inherent, phonon, and magnetic contribution. The example shows the total resistivity of single-crystal holmium in a-axis direction (Mark, that these considerations are only valid above Debye temperature).

ρ_0) and phonons (ρ_p). The former processes are temperature independent, the latter is proportional to temperature above Debye temperature (and proportional to T^5 below). In the case of rare earth metals, conduction electrons are coupled to the local spins via exchange. This leads to an additional scattering process and an additional contribution to resistivity ρ_m. According to sum rule for dc-resistivity (Matthiessen rule), the total resistivity ρ is just the sum of the different contributions: $\rho = \rho_0 + \rho_p + \rho_m$ [37]. They are depicted in figure 4.1 for the example of a holmium single crystal (measured in a-axis direction). The residual resistivity is determined from the low temperature saturation resistivity while the phonon contribution is extrapolated from the paramagnetic range. The magnetic lattice is regarded as periodic

potential in the same manner as the Coulomb potential of the ion cores is. In a perfectly ordered state (0 K) there is no local-moment contribution to resistivity. Only with increasing temperature, i.e. introduction of "magnetic dislocations" due to thermal motion, conduction electrons are scattered. In this regime, up to the ordering temperature, theory predicts a T^2 dependence for ferromagnets and and a T^4 dependence for antiferromagnets [37]. But the T^4 dependence in the case of antiferromagnets was not confirmed by measurements. Also in the case of holmium the resistivity obeys more the T^2 law in the antiferromagnetic regime. Above the ordering temperature spin-dependent scattering saturates. Its constant value in the paramagnetic phase is proportional to the De Gennes factor $(g-1)^2 J(J+1)$ [36]. At temperatures close to but above transition to an ordered magnetic state, spin fluctuations (sometimes refered to as paramagnons) can also contribute [37]. This effect leads to a deviation of the resistivity from linear behaviour in the low temperature range of the paramagnetic regime. Also band structure influences the magnitude of spin-disorder scattering and makes it strongly anisotropic. The saturation magnetic scattering is proportional to the projection of the Fermi surface to the respective direction of current. Much the same as the phonon contribution, magnetic scattering is isotropic in the a-b plane of the hexagonal lattice structure, but differs severely in the perpendicular c-axis direction. This corresponds to the rotational symmetry of the Fermi surface along c-axis. In c-axis resistivity there occurs a hump below Néel temperature. This feature is a manifestation of the magnetic superzones, that form due to the periodic, antiferromagnetic ordering in c direction.

Figure 4.2 shows resistivity measurements of single-crystal holmium in a- and c-axis direction, carried out in four point geometry (see figure 5.7). They are in good accordance with literature [54]. For precise absolute results, the holmium pieces were lapped down to a thickness of about 200 μm. The samples should be as thin as possible to ensure, that the whole sample profile contributes to conduction. Several hundred micrometres of material were removed, to get rid of dislocations due to the previous sewing.

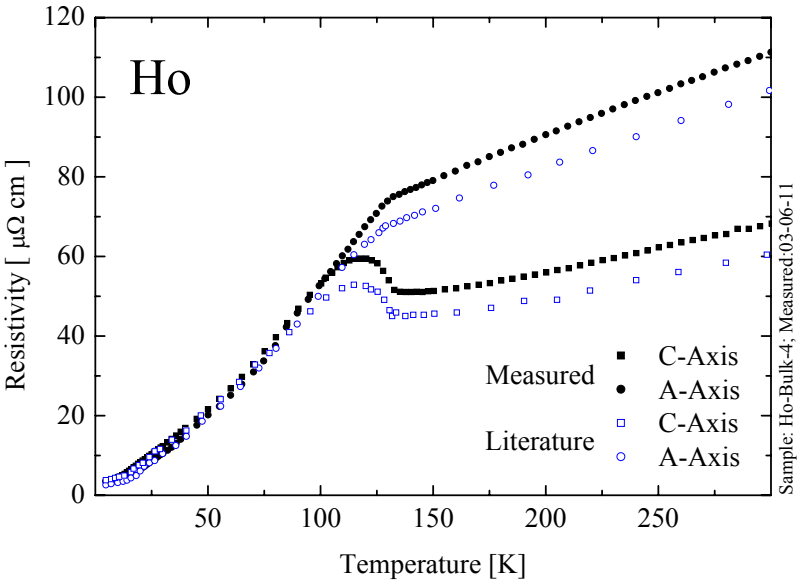

Figure 4.2: Resistivity of a holmium single crystal in a- and c-axis direction. The 0pen points denote earlier measurements by Strandburg et al. [54].

Even when magnetic scattering is taken into account, the resistivity of rare earths is still rather high, compared to other metals. This could be explained by a high probability of scattering from s-like into d-like bands. In the latter electrons experience an increased effective mass and contribute less to conduction [37]. Enhancement of the effective band mass can occur due to coupling with phonons, magnons, or due to interactions within the electron gas itself. Measurements and calculations estimate the electron mass enhancement due to phonons within the heavy rare earths to range around 35 % [70]. The total factor of mass enhancement was determined for gadolinium via de Haas-van Alphen effect (cyclotron masses) between 1.2 and 2.1 [71].

4.4.2 Optical Properties

Magnetic effects are also reflected in the optical properties of rare earth metals. At low frequencies the changes in magnetic scattering are expected to contribute in a Drude-like manner. Additionally, spin-wave excitations might be detected below 40 cm^{-1}/ 5 meV [55]. No measurements were carried out, up to now, on rare earth metals in this low frequency regime (below about 3000 cm^{-1}/ 0.37 eV).

A magnetic-phase dependent anomaly in optical spectra was observed at frequencies between 3000 cm^{-1}/0.37 eV and 5000 cm^{-1}/0.62 eV (depending on the atomic number). Below ordering temperature, an additional electron transition occurred and led to the formation of a peak. In the case of collinear ferromagnetism, like in gadolinium, this was interpreted in terms of s-f exchange splitting: In the exchange field of the ordered, localized 4f spins the conduction-electron bands are supposed to split, and in consequence, an excitation across the gap is to be expected. The very strong coupling of spin to orbital angular momentum makes this, otherwise forbidden, optical transition possible. In theoretical calculations on gadolinium, Nolting et al. [67, 68] distinguish between fully localized, and delocalized, "Stoner like", valence bands. The former ones are only exposed to local exchange. Their splitting should be temperature independent (as the magnetic moment at each site is). The latter ones experience an average exchange over a large volume and should show a temperature dependent splitting. Photoemission measurements by Kim et al. [62] and Schüßler-Langeheine et al. [63, 64] confirmed a temperature dependence for the Δ_2-band, as predicted. The latter also examined terbium, dysprosium and holmium. In contrast to gadolinium, those rare earths go through an antiferromagnetic phase, and already in this phase, they show the splitting. According to the theory, one would expect the splitting for delocalized bands to vanish in the antiferromagnetic phase, as the net magnetization is zero. The apparent contradiction is explained by a localization of the band wave function with respect to the c-axis direction, and a delocalization in the close-packed planes. A band splitting

in the discussed energy region, also for antiferromagnets, was already reported by optical means in the seventies (e.g. [29, 31]). Those results were interpreted in terms of the formation of periodic superzones, inducing a gap opening in the band structure, due to the periodic magnetic potential of the antiferromagnetic layers [30, 36].

Optical measurements on several rare earth metals were reported to confirm the previously discussed structure, for ferromagnets as well as for antiferromagnets. But most of them [29, 31] stretched only into the flank of the feature. Extensive measurements were presented by Weaver and Lynch in 1975 [32]. But they examined single crystals of the magnetic heavy rare earths only at 4.2 K, i.e. in the ferromagnetic phase. The peak, in question, was most pronounced for the elements of thulium and holmium. In 1991 Knyazev and Sandratskii [28] presented measurements at several temperatures, but only on gadolinium, terbium and dysprosium. They interpreted their results in terms of a temperature-independent splitting of d-like bands (i.e. associated with localized bands, according to Nolting [67, 68]).

Thus, in the context of this recent discussion, it was most tempting, to conduct detailed temperature- and field-dependent infrared/far-infrared measurements on holmium, the rare earth element with the most amazing variety of magnetic phases, with the largest magnetic moment per atom, and being among the least explored ones in this low-energy spectral region.

Chapter 5

Holmium Films

There are certain drawbacks associated with optical measurements on bulk-metal samples: As transmission through metals is nominally zero, only reflection measurements can be carried out. From those data, optical parameters have to be evaluated by the Kramers-Kronig formalism. This procedure introduces an additional source of uncertainty, due to the demand for extrapolation. Furthermore, there is a limit for reflection measurements to low frequencies: The high reflectivity of metal samples then approaches that of the reference mirror, and hampers precise results, especially at low temperatures. Although, with different optical means, a spectral range down to one wavenumber is accessible at our department, the high sample reflectivity limits measurements to frequencies above 50 cm^{-1}. Measurements on thin films in transmission geometry (including detection of phase shift) make the Kramers-Kronig formalism, as well as the reference mirror obsolete. The two gains would be to avoid the extrapolation uncertainty, as well as to extend the accessible frequency range to lowest energies. Furthermore, evaporation yields optically perfect surfaces, which do not need any further polishing. Drawbacks, on the other hand, are the difficulties in preparation, e.g. interaction with the substrate, while bulk single crystals are commercially available. Thus, the scope of this work was not only to explore the infrared optical properties of holmium bulk single-crystals. A further task was, to evaluate

the possibility of optical measurements on thin rare-earth films, and extend the range down to the limits of the far-infrared spectrum.

The following sections give a description of the techniques, used for the fabrication and characterization of holmium films. As rare earth metals show a certain tendency to react with other elements, some space is given to the discussion of interface problems. Nevertheless, it should be kept in mind, that holmium is much less reactive, than the light rare earths, like cerium or europium. Special care had to be spent on the choice of substrate, as it should not only satisfy the demands of a well ordered film growth, but first and foremost be suitable for optical measurements. The material of choice was silicon. Finally, characterization methods and their results are presented. X-ray diffraction, SQUID, and resistivity measurements demonstrated, that we are able, to produce films of holmium on silicon substrate in a quality of bulk polycrystalline material. The crystallites in the films are relatively large, and have a favourable orientation with their hcp planes parallel to the substrate surface.

5.1 Substrate Considerations

The task of optical measurements imposes certain restrictions on the film production, especially with regard to the choice of substrate. Due to the large skin depth of infrared radiation (see figure 6.14), not only in transmission, but also in reflection measurements, the optical properties of the substrate contribute. A standard technique for epitaxy of holmium and other rare earth films uses a sapphire substrate with two interlayers. On the (110) sapphire surface, several hundred Ångströms of niob are evaporated as a buffer layer. On top of the niob, a 100 nm thick layer of yttrium is deposited, presenting a good surface for the growth of (001)-oriented rare earth films [14, 12, 19]. Other groups report of direct evaporation of (001) holmium on a tungsten metal (110)-surface [13, 66]. These techiques are not feasible for optical transmission measurements, as substrate or interlayers are not

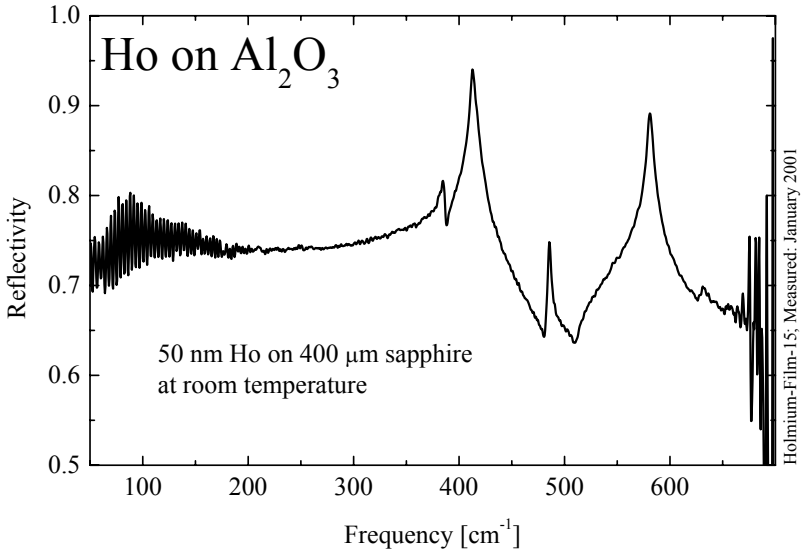

Figure 5.1: Reflectivity spectrum of a 50 nm thick holmium film on sapphire from 100 cm^{-1} to 700 cm^{-1} at room temperature. The pronounced phonon spectrum of the substrate is still visible through the film, and makes the measurements difficult to evaluate.

transparent. Even in reflection geometry, the contribution of the metallic substrate would pose severe problems. Any matching of the lattice constant becomes very difficult, usually utilizing a gradual change of composition in an alloy interlayer. Thus, the main focus for the right substrate had to be put on compatibility to the optical probing method, i.e. on transparency and on an easy-to-fit spectrum in the respective frequency range. In polar crystals, like sapphire, optically active phonons are excited. As figure 5.1 illustrates, they severely disturb the spectra in the infrared region. Shown there is the reflection spectrum of a 50 nm thick holmium film, evaporated on a sapphire single crystal.

The best choice, from the optical point of view, would have been diamond substrates. It has the best transparency of all possible materials in

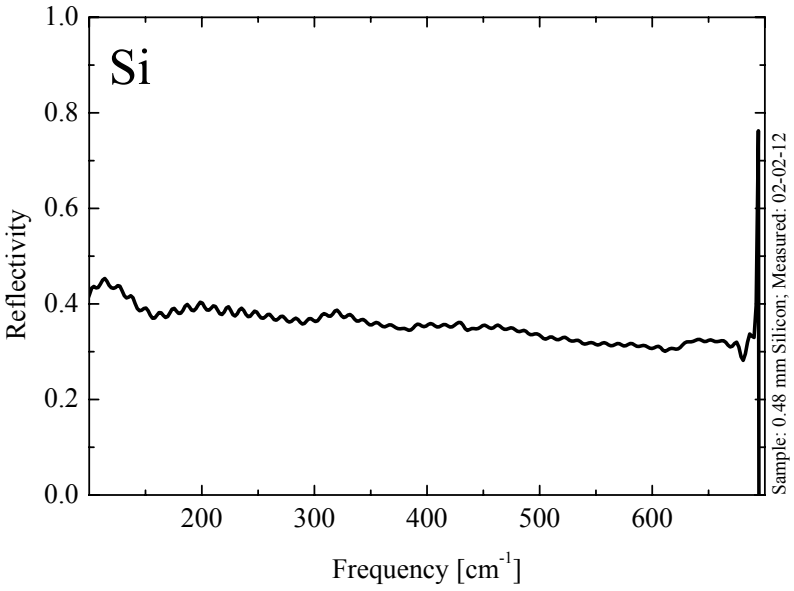

Figure 5.2: Reflectivity spectrum of a 480 μm thick silicon single crystal from 100 cm^{-1} to 700 cm^{-1} at room temperature. The frequency dependence is weak with no pronounced features.

the whole infrared spectral range. But for apparent financial reasons, the second best choice, a semiconductor single crystal, was finally used. In a semiconductor there are no disturbing optical phonon modes present. Thus, it is relatively easy, to calculate the pure holmium properties from measured data of holmium plus substrate. The most common, and thus cheapest, as well as best explored semiconductor is silicon. Its large band gap of 1.1 eV (8900 cm^{-1}) leaves the infrared spectral range mainly untouched. The infrared spectrum of a silicon single crystal substrate is plotted in figure 5.2. The zone-melted wafer, used for these experiments, was n-type phosphor-doped silicon, with a density of dopant atoms smaller than 10^{13} per cm^3. This corresponds to a resistivity of about 400 Ωcm. The substrate's (110) surface was first lapped with Al_2O_3 powder (grain size: 3 μm). Material of

100 μm thickness was removed, to get rid of dislocations due to the previous sawing process. Subsequently, chemical-mechanical polishing was applied with a syton solution (PH 11). Finally, the surface was cleaned in concentrated hydrochloric acid and dilute hydrofluoric acid. The substrate was mounted on a stainless steel substrate holder.

5.2 Interface Effects

There are two critical interfaces, that have to be considered, when dealing with thin rare earth films: The interface of film with substrate and the interface of film with air. The problem of exposure to air has to be taken into account, as the optical measurements, presented in the following chapter, could not be carried out in situ, under UHV conditions.

The oxidation kinetics of rare earth films, exposed to atmosphere, were examined by Burnham and Jameson [10]. At room temperature, they report a fast formation of oxide layers with thicknesses of two to three nanometres. This is about the saturation thickness of an oxide layer on aluminium. The pressures during their film preparation ranged between $1 \cdot 10^{-5}$ mbar to $1 \cdot 10^{-6}$ mbar and the qualitative statement was made, that the rate of oxidation depended on pressure during evaporation. We can confirm this observation, as holmium films of 50 nm thickness, evaporated at 10^{-5} mbar, became transparent within tens of minutes (for visible light), when exposed to air. On the other hand, when the pressure during evaporation was $1 \cdot 10^{-8}$ mbar or better, films of the same thickness were virtually stable on exposition to atmosphere. For the case of the rare earth gadolinium, Weller and Sarma [21] even observed the formation of a passive layer just like on aluminium. As the oxides of rare earth metals have a relatively high transparency [15], and as they are thin, compared to the skin depth (see figure 6.14) of infrared radiation in a metal, the influence on the optical spectra is small, even at frequencies around phonon absorption lines. In the case of severer problems for very thin films it is still possible, to evaporate a cap layer of silicon on

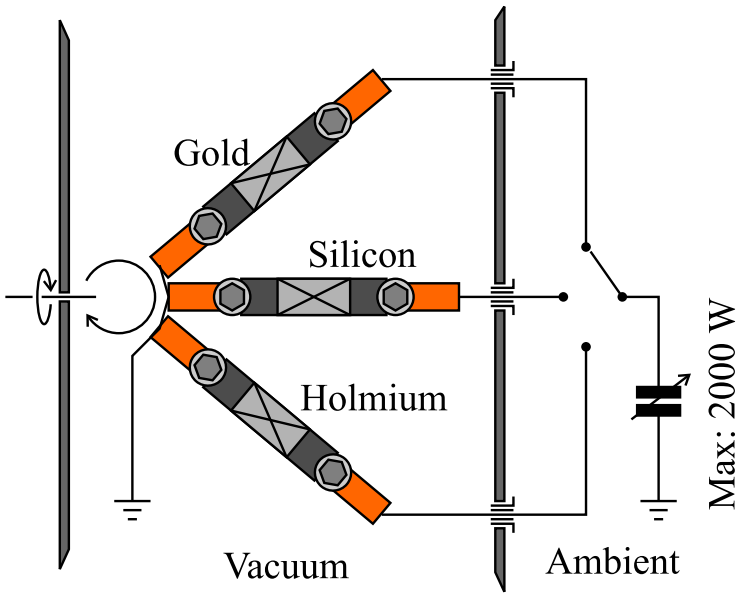

Figure 5.3: The three boats of the evaporator were mounted on a turn table with flexible electric contacts, to move them properly beneath the substrate (top view).

top of the films to protect them against oxidation.

The interface of rare earth films with the substrate also has to be taken into account. It is a well known fact, that the rare earth metals like to get entangled with their substrate. For that reason one usually introduces a buffer layer between rare earth film and substrate [12]. But this buffer layer uses to be some highly melting metal, and is, thus, unsuitable for optical (especially transmission) measurement. The rare-earth-silicon interface is problematic. It was reported, that at annealing temperatures above 350 $°C$ even rare earth films of several hundred nanometres completely react to silicides within 15 minutes [18, 20]. Thus, the annealing of such films has to be considered with care and annealing temperature has to be kept as low as possible.

Symbol	a[nm]	c[nm]	Melting Point [$°C$]	Point of Sublimation [$°C$]
Gd	0.36336	0.57810	1311	398
Tb	0.36055	0.56966	1360	389
Dy	0.35915	0.56501	1409	290
Ho	0.35778	0.56178	1470	301
Er	0.35592	0.55850	1522	317
Tm	0.35375	0.55540	1545	232

Table 5.1: Lattice constants, melting points and points of sublimation for the magnetic heavy rare earth metals [73, 46].

5.3 Deposition and Annealing

Neither was the aim of this work a fabrication of film thicknesses in the range of monolayers. A thickness around 50 nm yields sufficient transmitted intensity for optical measurements. Nor was, for previously discussed reasons, the substrate matched for epitaxial growth. Thus, the method of choice for deposition of the rare earth films was evaporation by resistance heating. This rugged technique is capable of evaporating large amounts of highly melting materials. Table 5.1 shows melting point and point of sublimation of the heavy, magnetic rare earth metals. Although sublimation already starts at pretty low temperatures, the melting point is rather high. For evaporation, 99.9 % pure holmium pieces were cut to flat cuboids. The metal was evaporated from a tungsten boat, which was, via electrical feedthroughs, connected to a high-current tunable source (maximum 5 V, 400 A, ac). The usual current during evaporation was about 100 A. The power feed-throughs were cooled with liquid nitrogen, to diminish heating and subsequent increase in pressure during evaporation. For a constant evaporation rate, it was necessary to completely melt the holmium block once. Otherwise, heat transfer from boat to holmium was badly fluctuating, when partial melting of the block changed the contact surface. The extreme heating (under UHV conditions) then also removed the more volatile contaminations from the

evaporation material. Thus, there was the need for sufficient power not only to reach the sublimation point, but to completely melt the lump of holmium. The evaporator was designed with three boats, each to host a different material. In this way, it is possible, to evaporate gold contacts on top of the rare earth films for dc characterization, as well as to cover films with a (transparent) protection layer against oxidation. The three boats were mounted on a turntable with flexible electrical contacts, to move them right beneath the substrate, i.e. the shutter. In this manner the distance between the boats was maximized, to prevent contamination of the rare earth metal boat with the neighbouring materials (see figure 5.3). Different masks were moved in front of the substrate, to allow for an in-situ change of the evaporated structures according to the current function of the layer (e. g. square for the rare earth film, four stripes for the four-point probing, large square for cover layer).

It was possible to heat the block of the substrate holder up to 300 °C. A PT-500 temperature sensor was mounted next to the substrate. The heater consisted of a tungsten-rhenium alloy, coiled up on two parallel quartz rods. They were mounted above the substrate holder in a distance of 20 mm, to heat it via radiation from the back. The transformer supplied a maximum power of 110 W (22 V, 5 A) and the heater resistivity was 4.4 Ω. After evaporation at room temperature, the films were annealed at relatively low temperatures (below 200 °C) for several hours.

Hentzell et al. [11] measured the grain size of metallic 100 nm thick films in dependence of the substrate temperature during evaporation. They report very small grain sizes below 20 nm, when the substrate temperature was around one fifth of the metal's melting point. In contrast to their procedure, we evaporated on a room temperature substrate with subsequent annealing at relatively low temperatures for several hours. At temperatures below 300 °C (one fifth of the melting point of holmium) we achieved large grain sizes of about 500 nm. For rare earth metals this procedure is recommendabe, as reactivity strongly increases with temperature, even affecting films under

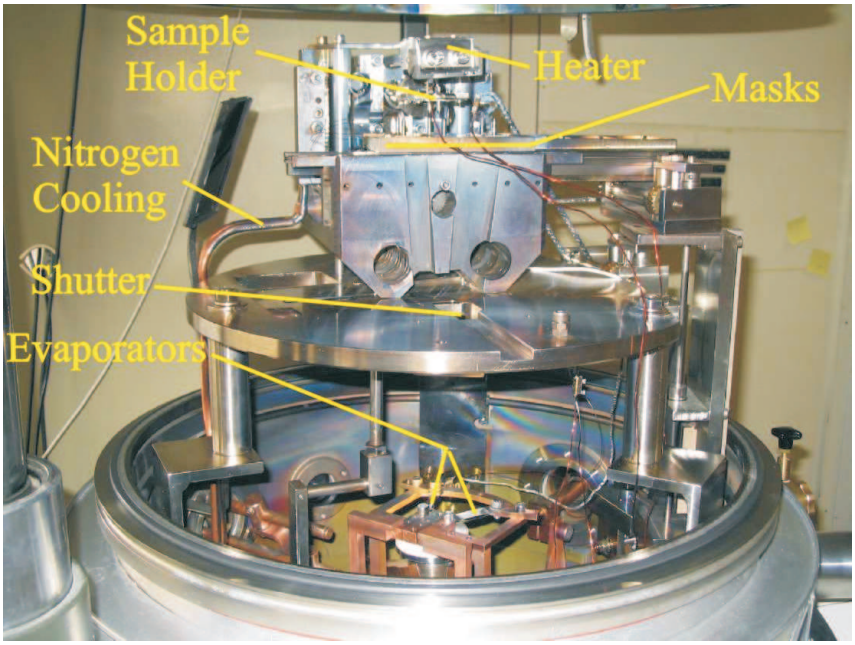

Figure 5.4: This photograph shows the interior of the UHV chamber.

UHV conditions.

5.4 The Vacuum Chamber

The vacuum chamber formerly was part of a Balzers UMS 500 evaporation system. The large bell provided plenty of space for the necessary fixtures, and the automatic timer for heating and water cooling of the bell was very comfortable to quickly gain low pressures. The pneumatically liftable bell allowed a fast and spacious access to the interior of the chamber. A Pfeiffer DUO 030 rotary pump, and a Pfeiffer TMU 521 P turbo-molecular pump provided enough pumping power to reach a base pressure of $1 \cdot 10^{-8}$ mbar within less than 36 hours. The end pressure of $1 \cdot 10^{-9}$ mbar was reached by evaporating holmium as getter substance, and by cooling a getter surface within the chamber to liquid-nitrogen temperature. Usually it was possible to keep the pressure below $5 \cdot 10^{-9}$ mbar during film evaporation. This was

achieved by cooling the electrical feedthroughs of the evaporator with liquid nitrogen. Pressure was measured with a Balzers IKR 060 cold cathode tube and a Balzers TPG 300 pressure gauge. Determination of the film thickness was achieved by a quartz scales inficon IC6000. It was calibrated by thickness measurements according to the Tolansky method [17].

5.5 Holmium Film Characterization

Evaporation of holmium was carried out at pressures between $2 \cdot 10^{-9}$ mbar and $1 \cdot 10^{-8}$ mbar. The evaporation rate was kept constant at about 1 Å per second. Heating of the evaporator did not affect the substrate temperature noticeably: The substrate temperature during evaporation stayed constant at room temperature. Some of the samples were annealed at different temperatures after evaporation. Characterization of the samples was accomplished by x-ray diffraction, SQUID, and resistivity measurements to give evidence of purity, crystallite size, and crystallite orientation.

5.5.1 X-Ray Diffraction

To evaluate the quality of the evaporated holmium films, x-ray diffraction measurements were carried out [1]. Small-angle x-ray (SAXR) diffraction was applied, to verify the in-situ thickness measurement of the quartz scales. The oxide layer thickness on top of the films was estimated to be about 2 nm, even after days of exposure to air. As expected, the films were polycrystalline. Domain sizes were estimated by the Scherrer formula. For annealed films, they were in the order of the film thickness (thickness 100 nm; domain size: about 60 nm).

Measurements in Bragg-Brentano geometry showed a preferred orientation of the crystallites' crystallographic c-axis direction perpendicular to the substrate plane. Figure 5.5 shows the pronounced peak of the (002) planes

[1] By: Stephan Hirschmann, Kristall-Labor, Universität Stuttgart

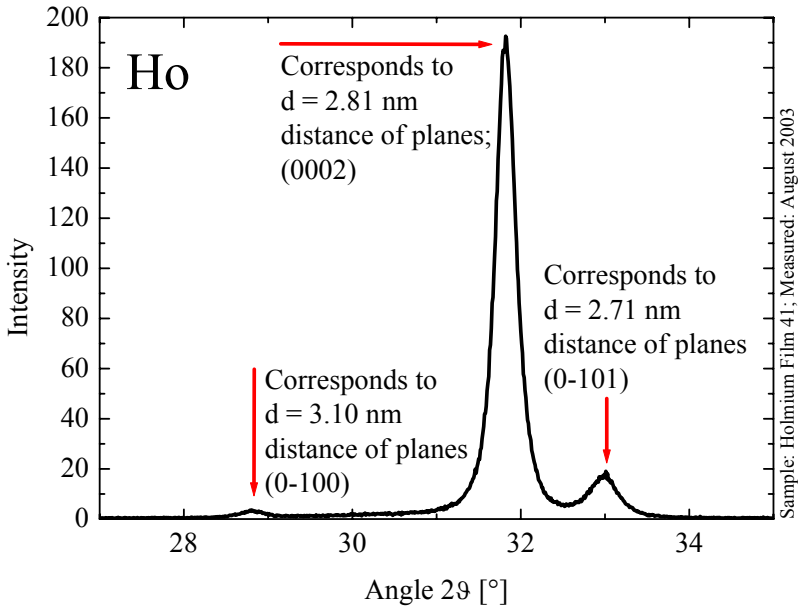

Figure 5.5: Bragg-Brentano scan of a holmium film. The most pronounced peak is related to the hcp basal planes. The sample thickness was 1100 nm and it was annealed at 110 $°C$ for 18 h.

in the holmium hcp lattice. The width of the rocking curve indicated an average deviation from that mean direction of about 5 ° for well aligned films [22, 23].

5.5.2 SQUID Magnetometry

Several film samples were examined in a SQUID magnetometer (Quantum Design MPMS XL). The saturation magnetization reveals information about the major orientation of crystallites within the film, as well as its purity. As the results of Strandburg et al. [54] show (see chapter 3.3), in-plane and out-of-plane magnetization differ severely for holmium single crystals. Figure 5.6 shows the results for a film of 330 nm thickness. In these measurements, the direction of the applied field was parallel to the film. The set of curves

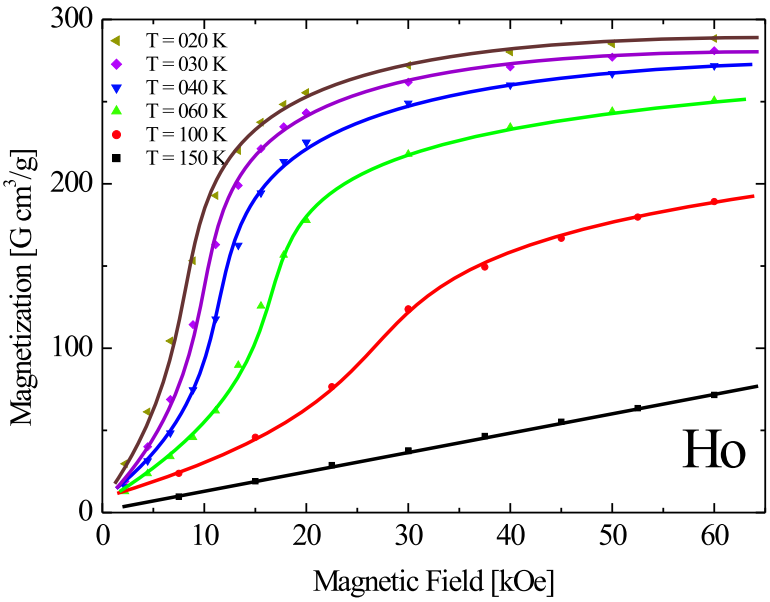

Figure 5.6: Magnetization curves of an evaporated holmium film. The field direction is parallel to the film plane. The saturation magnetization approaches values, characteristic for the in-plane magnetization of a single crystal.

resembles Strandburg's results for a single crystal with field applied perpendicular to the c-axis direction. This fact, and especially the high saturation magnetization of 300 G cm^3/g give clear evidence, that a majority of the crystallites is well oriented with their c-axis heading perpendicularly out of the film plane.

5.5.3 Dc Resistivity

Furthermore, the film quality was judged by the help of dc-resistivity measurements between 4.2 K and 300 K. These measurements were carried out in four-point probe geometry. The advantage of this method is, that the contact

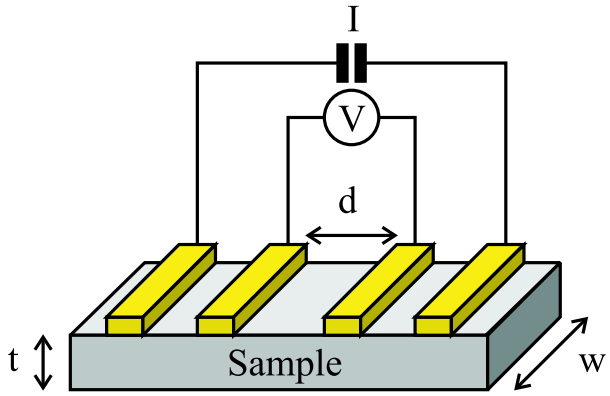

Figure 5.7: Dc-characterization was carried out in four-point probe geometry. As contacts, four parallel gold contact stripes were evaporated on top of the sample.

and lead resistances do not account (no current flows through the high resistivity voltmeter; see figure 5.7). After their fabrication, the holmium films were covered in-situ with four gold contact stripes. Then the samples were mounted on a sapphire crystal (for good thermal conduction), connected to a plug by gold wires and silver paint, and finally mounted on a sample rod in the cryostat.

The specific resistivity of the film calculates from the measured resistance R (i.e. the ratio of the measured voltage U to the injected current I), the distance of the inner two contacts d, and thickness t and width w of the sample(see figure 5.7):

$$\rho = \frac{U}{I}\frac{t \cdot w}{d}. \tag{5.1}$$

The ratio of resistivity at 4.2 K and at 300 K is widely used, to characterize the impurity and dislocation concentration within crystalline samples. But there is a lot more of information, especially for magnetic rare earth samples, to be extracted from temperature dependent resistivity measure-

ments. In the paramagnetic range above 133 K, the slope of the resistivity curve is only governed by phonon scattering. A different amount of dillute contaminations and dislocations in the film will only result in a parallel shift of the curve (temperature independent contribution). Thus, different slopes of different samples would indicate errors in the assumed sample geometry, which should be mainly due to errors in the film thickness determination ($\pm 10\%$). Around Néel temperature, the resistivity curves in, and perpendicular to the crystal planes differ dramatically (see figure 4.2). The hump, that occurs only in c-direction, is a good measure for the crystallite's alignment. The less pronounced the hump is, the more crystallites are aligned with their hcp-basal planes within the film plane. The temperature range below Néel temperature is difficult to describe theoretically, as it is a superposition of temperature dependent phonon and magnetic scattering (see chapter 4.4.1). But at lowest temperatures, both temperature dependent contributions are frozen out, and then, the resistivity is mainly due to contaminations and dislocations (being a good measure for their concentration).

Figure 5.8 shows resistivity measurements of the used bulk evaporation material (polycrystalline), and of four films, which were annealed at different temperatures. The curve for the polycrystalline bulk sample coincides well with the data according to Strandburg et al. [54]. The grains have a size, where further enlargement does not improve conductivity anymore (because they are large against the free path of the electrons).

The evaporated holmium films show higher absolute resistivity values, than the bulk material does. This is to be expected, as grain boundaries accumulate during condensation on the cold substrate (room temperature). But, as the curves in figure 5.8 show, the grain size can be enlarged by annealing. For an annealing temperature of 180 °C (annealing time: 6 h, down triangles) the absolute resistivity well approaches the saturation values (diamonds). The film thickness was 100 nm, and the pressure during evaporation ranged between $5 \cdot 10^{-9}$ mbar and $9 \cdot 10^{-9}$ mbar. The hump feature at the magnetic phase transition is observed for all curves, indicating a consider-

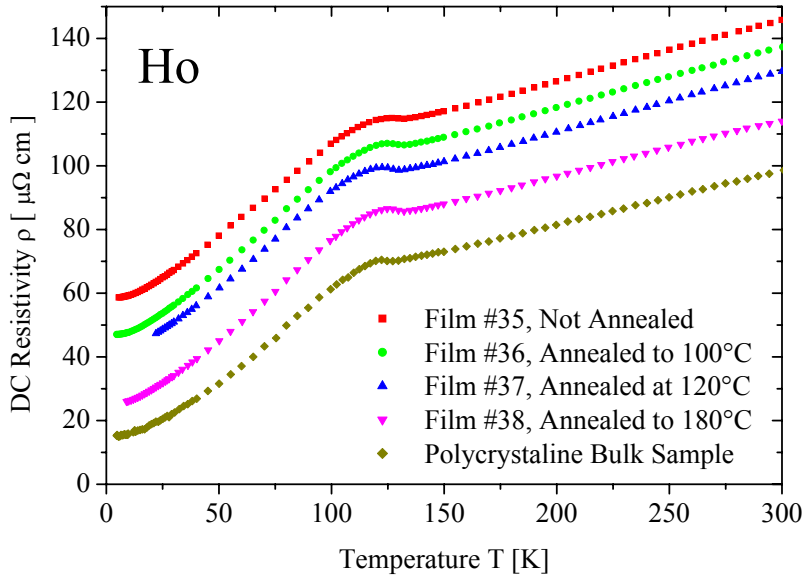

Figure 5.8: Four polycrystalline holmium films of 1000 Å thickness were annealed at different temperatures. The increasing size of the crystallites is reflected in a decrease of resistivity.

able amount of crystallites having their hcp-basal planes tilted out of the film plane (and thus, c-axis conduction contributes).

5.6 Results of Film Characterization

The temperature dependent resistivity measurements on holmium films confirm, that the technique of low-temperature ($< 200\ ^{\circ}C$) annealing for several hours can greatly enlarge the grain size within the films. The absolute, specific resistivity of the films approaches that of the pure bulk material, indicating a low contamination of the film. A further evidence of sufficient film purity is the high saturation magnetization, measured in the SQUID magnetometer. With a value of around 300 G cm^3/g it resembles that of

bulk single crystals. In particular, this high value shows, that a considerable part of the crystallites is lined up with their hcp-basal plane along the film plane. X-ray diffraction measurements confirm this preferred orientation and determine the crystallite size to be around 600 nm. An oxide layer on top of the films was estimated to be around 2 nm thick, even after hours of exposure to atmosphere. This result is of particular interest for optical measurements, as the skin depth of infrared radiation into a rare earth metal is orders of magnitude larger. Thus the surface contamination will only negligibly contribute to the optical spectra (even in the range of phonon absorption), in contrast to surface sensitive measurements, like photoemission spectroscopy. As the infrared results, presented in the next chapter, confirm, it is well possible to fabricate reproducible samples for optical measurements by vapour deposition plus annealing.

Chapter 6

Infrared Measurements on Holmium

The infrared range of the electromagnetic spectrum is located between the visible and the microwave region, i.e. between about 10 cm^{-1} (1.2 meV) and 13000 cm^{-1} (1.6 eV). In terms of wavelength, this is the region from 750 nm to 1 mm. It was already pointed out in the previous chapters, that low energy spectroscopy is a fertile field with regard to electron transport in matter. Continuous and minute excitations of electrons in closest vicinity to the Fermi surface can be well explored. For the heavy rare earth metals, exactly these electrons play the crucial part in mediating the magnetic exchange interaction. Thus, the complex ordering, especially in holmium, will have a distinct influence on the infrared and far-infrared optical spectra of the material.

One standard technique for the determination of optical parameters is ellipsometry. Several publications on optical data of rare earth metals utilized this method [28, 31, 29]. But ellipsometry is limited by the fact, that, at low frequencies, the extinction ratio of the available polarizers does not meet the requirements anymore. An alternative method, that is able to further push the frontier to lower frequencies, is Fourier-transform infrared (FTIR) spectrometry. In principle, the accessible frequencies cover the range from

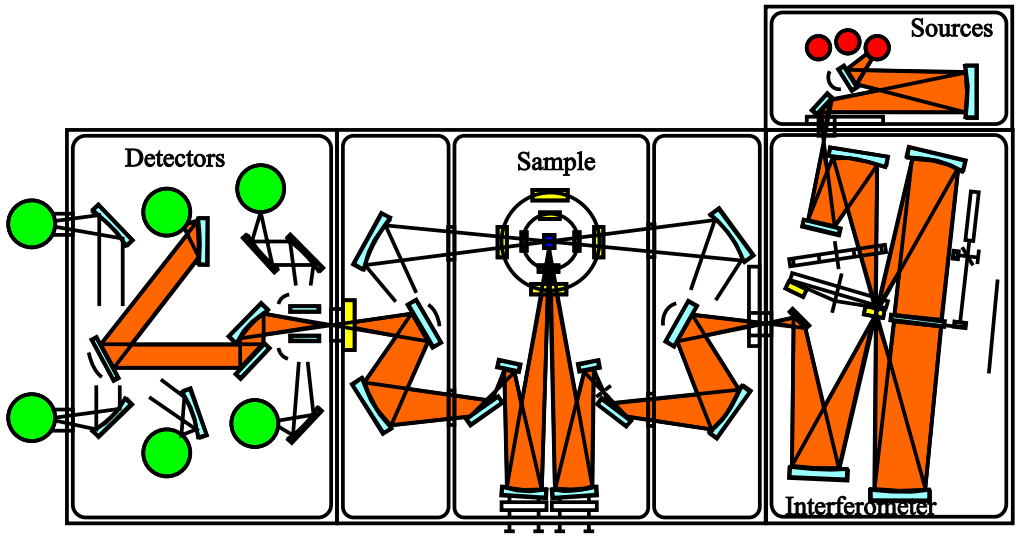

Figure 6.1: Setup of the modified Bruker IFS 113v Fourier transform infrared spectrometer (FTIR).

10 cm^{-1} up to 10000 cm^{-1}. The first section of this chapter gives a brief description of the spectrometer, that was used. In the second section, measurements on bulk single crystals are presented. For the low-frequency range (below 1000 cm^{-1}), the Drude free-electron contribution and some low energy transitions are discussed, while for the high-frequency range, a focus is put on the magnetic feature around 3000 cm^{-1}. It is often referred to as exchange splitting, and occurs below holmium's Néel temperature of 133 K. As this feature strongly depends on the magnetic order of the sample, spectra were also taken in a variable external magnetic field. As already stated in the previous chapter, optical measurements on evaporated films bear several advantages. In the third section of this chapter, spectra will be presented, which were measured on film samples. These experiments confirm the feasibility of infrared optical measurements on holmium films.

6.1 The Fourier-Transform Spectrometer

The Fourier-transform infrared spectrometer, used for the presented measurements, is a modified Bruker IFS 113v. It is capable of measuring reflectivity as well as transmittivity spectra from 10 cm^{-1} to 10000 cm^{-1}. For a detailed description of infrared spectroscopy and Fourier-transform technique see, for example, the textbooks of Griffiths and de Haseth [6], or Möller and Rothschild [9].

In an optical cryostat (CryoVac) the sample temperature can be continuously tuned from 2 K up to room temperature. Alternatively the sample can be mounted in a cryostat (Oxford SpectroMag4000) which allows to apply magnetic fields up to 8 T. The field can be arranged either perpendicular to, or in direction of the field. The accessible temperatures of this cryostat also range from 2 K to room temperature. The sample can be moved within the cryostats to be replaced by an aluminium reference mirror (5000 Å evaporated on glass substrate).

To cover the whole frequency range, there are three light sources available, as well as four detectors. The sources are a tungsten lamp for the near-infrared range (2000 cm^{-1} to 10000 cm^{-1}), a globar lamp for the mid-infrared range (500 cm^{-1} to 7000 cm^{-1}), and a mercury-arc lamp for the far-infrared range (10 cm^{-1} to 700 cm^{-1}) [7].

The far-infrared radiation is detected by a liquid-helium cooled bolometer (at 4.2 K) and a pumped, liquid-helium cooled bolometer (at 1.2 K) [4]. In the near- and mid-infrared region, an indium antimonide (InSb, at 77 K) and a mercury-cadmium telluride (MCT, at 77 K) detector are used respectively [8].

The optical elements also have to be adopted over the whole frequency range. In the Michelson interferometer, different beam splitters are available: Quartz glass for the near-infrared, potassium bromide (KBr) for the mid-infrared, and different thicknesses of mylar foil in the far-infrared region. The polarizers for near- mid- and far-infrared are made from quartz glass, KRS, and Polyethylene respectively. The material of the windows in the op-

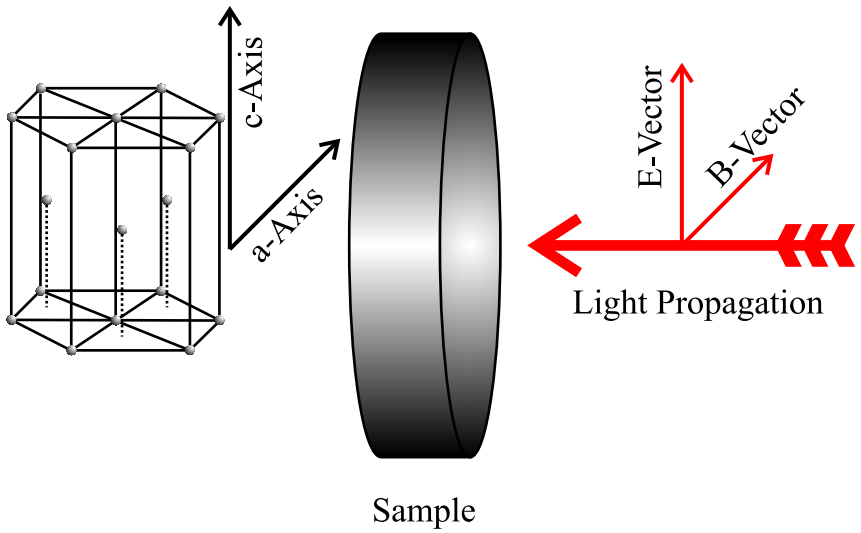

Figure 6.2: Geometry of sample and light polarization. To switch between the two polarization measurements (E parallel to c or a axis) polarization is turned for 90 °. The sample is left untouched.

tical cryostats is either polyethylene in the far-infrared range, or Zinkselenide (ZnSe) in the mid- and near infrared region.

Data acquisition is managed via PC. The programme Opus, delivered by Bruker, carries out the fast Fourier transform [6]. All holmium samples, the bulk single-crystals as well as the films, were measured in reflection. Thus, the optical parameters of conductivity and dielectric constant have to be calculated via Kramers-Kronig analysis of the measured spectra [5].

6.2 Measurements on Bulk Single Crystals

In this section, the results of reflection measurements on holmium single crystals are presented. The measurements were carried out temperature dependent in the previously described Fourier Transform Infrared Spectrometer (FTIR). Polarized light was used, with the plane of polarization being either parallel to the crystallographic c-axis or parallel to the crystallographic a-

axis direction. Thus, the answer of the valence and conduction electrons to an ac field is probed, stimulated either within the hcp basal planes, or perpendicular to the basal planes. As discussed in sections 4.4.1 and 4.4.2, there are some distinct differences to be expected in the spectra, depending on the direction of polarization. In addition to the different symmetries and different lattice parameters, there occurs a magnetic superstructure, which is periodic in c direction but uniform within each basal plane (see chapter 3.3). The antiferromagnetic helical phase forms below the Néel temperature of 133 K and below the Curie temperature of 20 K the ferro-cone helix is established.

6.2.1 Reflectivity Spectra

Figure 6.3 shows the frequency dependent reflectivity of single-crystalline holmium on a logarithmic scale. The measurements were carried out from 50 cm^{-1} to 10000 cm^{-1} covering four decades. The geometry of the setup is sketched in figure 6.2. By turning a polarizer in front of the sample, the probing E-Vector can be changed by 90 °, to switch between a-axis and c-axis orientation. In both directions of polarization, there develops a pronounced feature below Néel temperature. As it was observed for gadolinium, terbium, and dysprosium [28], also in these measurements on holmium, the feature is much more prominent for the c-axis polarization direction. The insets enlarge the region around that magnetic feature. At low frequencies, below 1000 cm^{-1}, there occur some temperature dependent changes in the spectra, which indicate additional contributions,to the free-electron Drude behaviour. This gives evidence of some low-energy excitations between 100 cm^{-1} and 500 cm^{-1} (see also: arrows in the insets of figure 6.5).

6.2.2 Extrapolation and Fit of Reflectivity Data

A Kramers-Kronig analysis of the measured reflectivity data yields the optical conductivity spectrum. The wide range of measured data over four decades

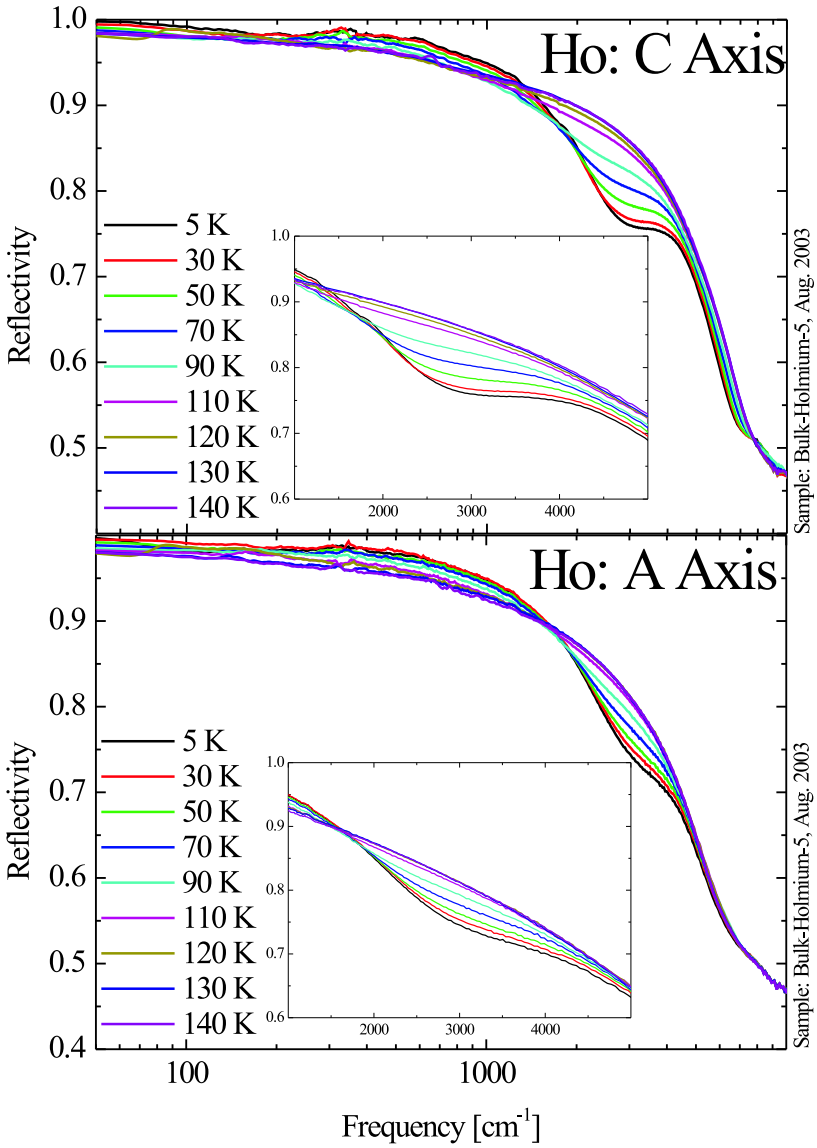

Figure 6.3: Reflectivity of single-crystalline holmium in the far-, mid-, and near-infrared spectral range. The direction of polarization was parallel to a axis and c axis respectively.

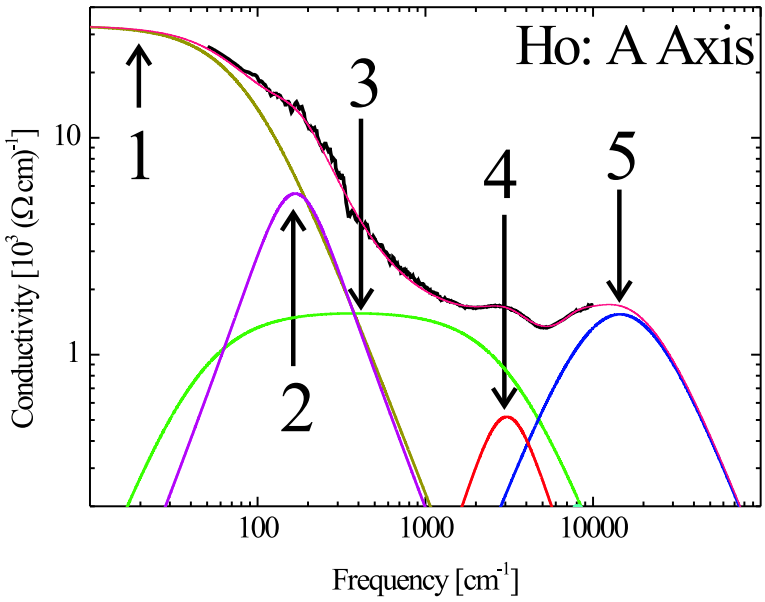

Figure 6.4: Illustration of the fitting and extrapolation, here in the case of holmium in a-axis direction at 70 K. The thick line shows the conductivity, calculated from measured reflectivity data. The least square fit to the measured data (thin line) consists of the Drude free-electron model (curve 1), and several Lorentzian oscillators (curves 2 to 5), representing transitions between localized states.

makes the Kramers-Kronig formalism a reasonable tool. Still, some care has to be spent on the extrapolation to low and high frequencies. The measured data are fitted, as well as extrapolated, by the help of the Drude-Lorentz model (see chapter 4 and figure 6.4). For frequencies below 50 cm^{-1}(beyond the measured data), a Drude-like behaviour was assumed (curve 1). The measured dc-conductivity (figure 4.2) was put into the model as fixed parameter (yielding the plasma frequency of the Drude model; equation 4.7), while the scattering rate was used as free parameter, to fit the model to

the measured low frequency data. At high frequencies, above 10000 cm^{-1}, a broad interband transition was assumed in the shape of a Lorentzian oszillator (curve 5). This feature was observed in optical measurements for several rare earth metals [32, 27], and in the case of holmium, it was located arround 14500 cm^{-1} [29]. At much higher frequencies, there are no transitions of valence electrons any more. And thus, the optical conductivity approaches zero above the interband peak at 14500 cm^{-1}. Low and high frequency extrapolations were used, to fit (least-square fits) the measured data in between self consistently. To fit the data properly with the Drude-Lorenz model, further contributions (in addition to the low-frequency Drude extrapolation and the high-frequency interband oscillator) had to be introduced: The first, being the one of major interest, is a strongly temperature dependent peak around 3000 cm^{-1} (curve 4). It is related to the formation of the antiferromagnetic phase, and its temperature dependence is subjected to further discussion later. The next two oscillators, less temperature dependent, are located between 100 cm^{-1} and 500 cm^{-1} (curves 2 and 3). They can be contributed to the increased density of states in the close vicinity of the Fermi energy, due to a hybridization of inner, 4f electrons with band electrons [72]. A further oscillator was introduced around 10000 cm^{-1}, to improve the fit. But it is only an artefact, due to the linking of measured, and extrapolated data in this spectral region. Its magnitude is negligible, compared to the other contributions (and thus, it is not to be seen in figure 6.4). Finally, the measured reflectivity data, together with the fitted extrapolations at low and high frequencies (ranging then from 0.1 to 1000000 cm^{-1} in total) were subjected to the Kramers-Kronig formalism, to yield the frequency dependent conductivity curves. Figure 6.4 shows, exemplarily for 70 K data in a-axis polarization, the conductivity, calculated from the measured data (plus extrapolation) as bold line, as well as the least square fit (thin line), together with its contributions (curves labelled 1 to 5).

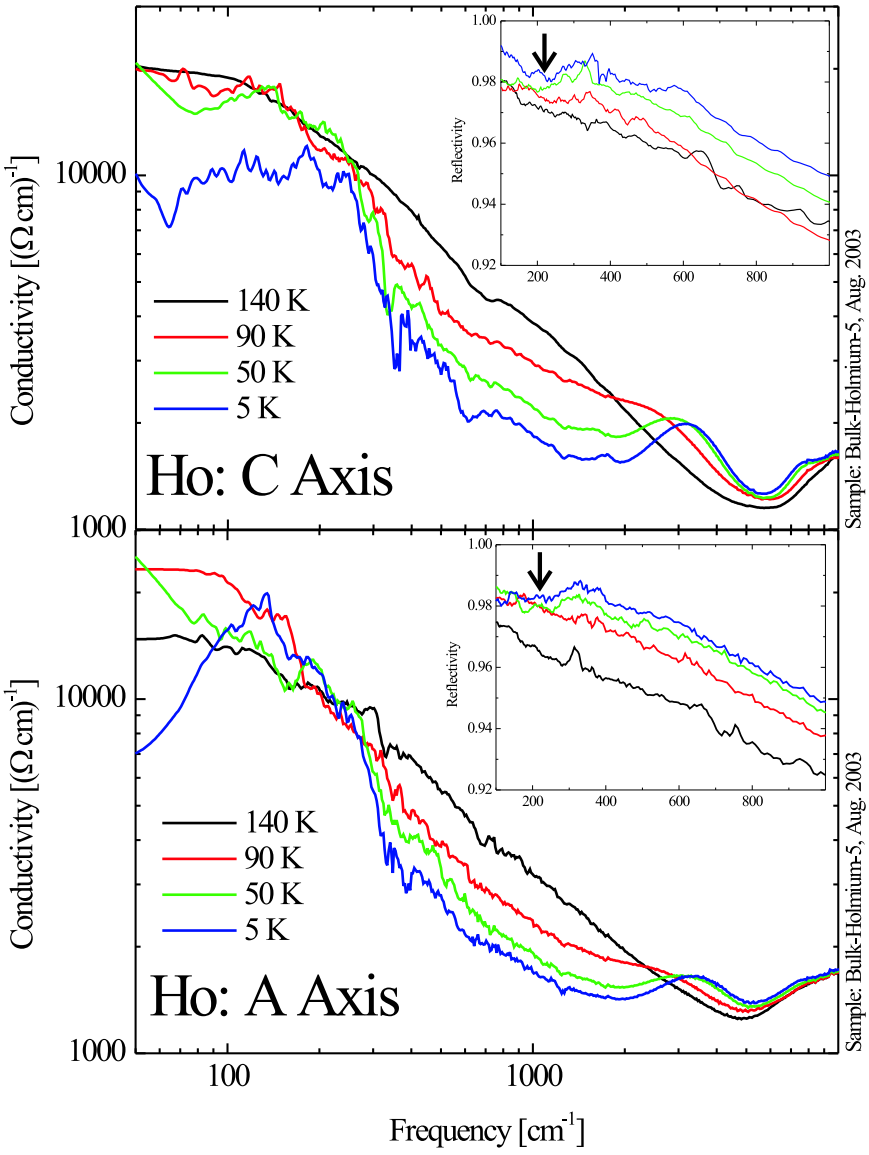

Figure 6.5: Conductivity of single-crystalline holmium on a logarithmic scale. The direction of polarization is parallel to a-axis and c-axis direction respectively. The inset illustrates the low-frequency changes in the original reflectivity spectra with decreasing temperature (arrows).

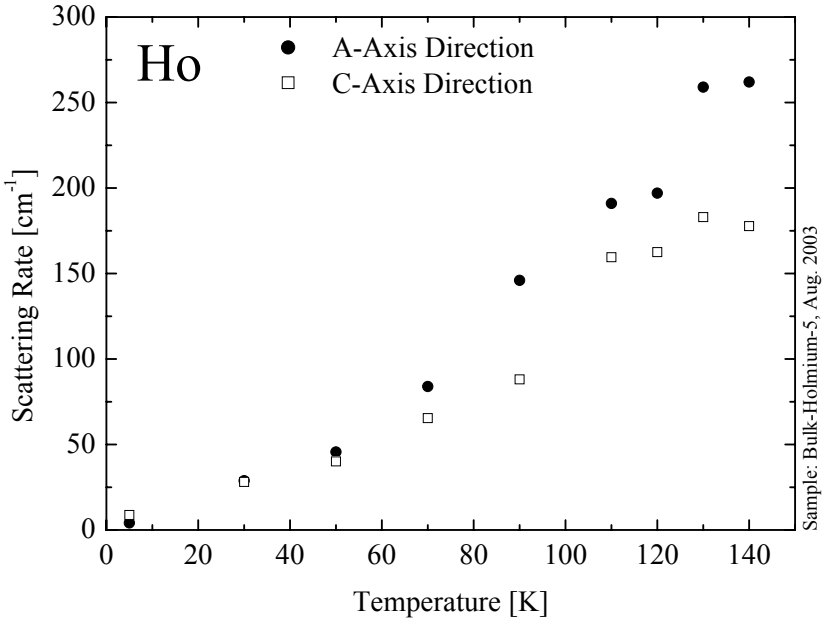

Figure 6.6: Scattering rate of the completely free conduction electrons, according to the Drude-model low-frequency fit.

6.2.3 Far-Infrared Conductivity

Reflectivity measurements were carried out down to 50 cm^{-1}. At lower frequencies, this technique meets its limitations, as the sample's reflectivity approaches that of the reference mirror. Unless this results in an increasing uncertainty at the low-frequency end of the measured spectra, there is clear evidence in reflectivity data, indicating a temperature dependent dip around 200 cm^{-1} (see insets of figure 6.5, arrows). The logarithmic scale of figure 6.5 emphasizes the far-infrared part of the calculated conductivity spectra. Shown are the curves for 140 K in the paramagnetic phase, for 90 K and 50 K in the antiferromagnetic phase, and for 5 K in the ferromagnetic phase. In the conductivity plot, one can clearly identify the Drude tail (feature 1 in figure 6.4). Its flank continually retreats to lower frequencies with decreasing

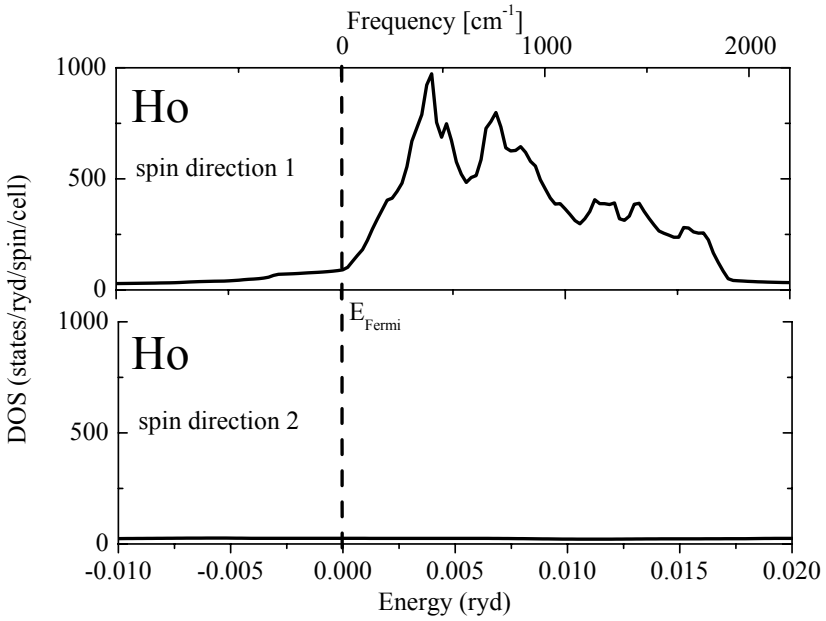

Figure 6.7: Calculated density of states, according to self-interaction-corrected local-spin-density approximation [72](see also [69]).

temperature, indicating the decreasing scattering rate of the free electrons, due to temperature dependent magnetic and phonon scattering. Figure 6.6 shows the temperature dependence of the free electron scattering rate. The results at lowest frequencies reveal, that, at temperatures below 130 K, there develops an additional transition in the flank of the Drude free electron contribution. With the retreat of the Drude flank, this feature becomes more and more pronounced (feature 2 in figure 6.4).

Calculations of H. Winter [72] (according to self-interaction-corrected local-spin-density approximation, see e.g. [69]) for the density of states of holmium at zero Kelvin predict an increased density of states just above the Fermi niveau, as depicted in figure 6.7. These states occur due to hybridization of an inner 4f level with outer valence niveaus. They may explain the unusual transitions at these low frequencies.

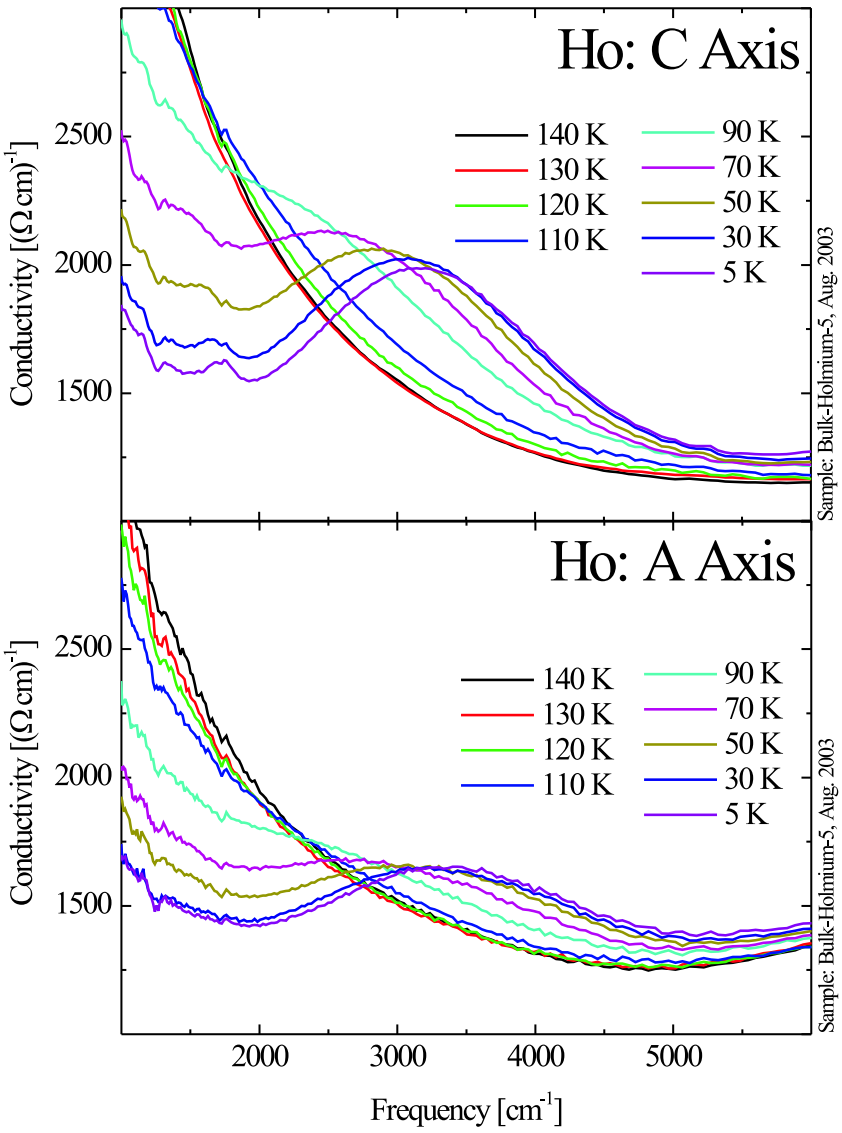

Figure 6.8: Optical conductivity of a holmium single crystal in the range of the magnetic peak. The upper graph refers to measurements with the E-vector in direction of the c-axis, while for the lower graph, the E-vector was lying within the planes of the hcp lattice.

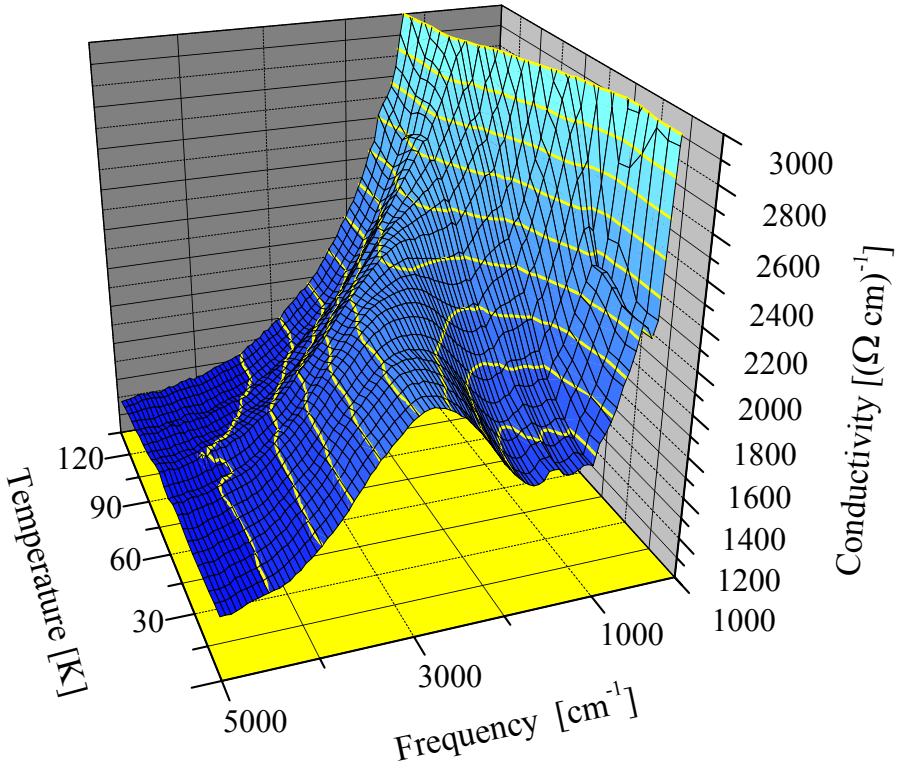

Figure 6.9: 3-d plot of the temperature-dependent optical conductivity of a holmium single crystal around the magnetic peak. The probing light was polarized parallel to the c-axis direction of the crystal.

6.2.4 Mid-Infrared Conductivity

The most striking feature in the spectra of holmium occurs in the mid-infrared spectral region. As clearly to be seen in figure 6.3, there exists a temperature-dependent excitation at about 3000 cm^{-1}. This feature appears together with the formation of the antiferromagnetic phase, i.e. below 133 K. As already discussed in section 4.4.2, it is interpreted in terms of a splitting of valence-electron bands, due to the exchange field of the ordered 4f-electron local magnetic moments.

The evaluated, frequency-dependent conductivity of single- crystalline holmium is depicted in figure 6.8. Again, the two graphs refer to the E-

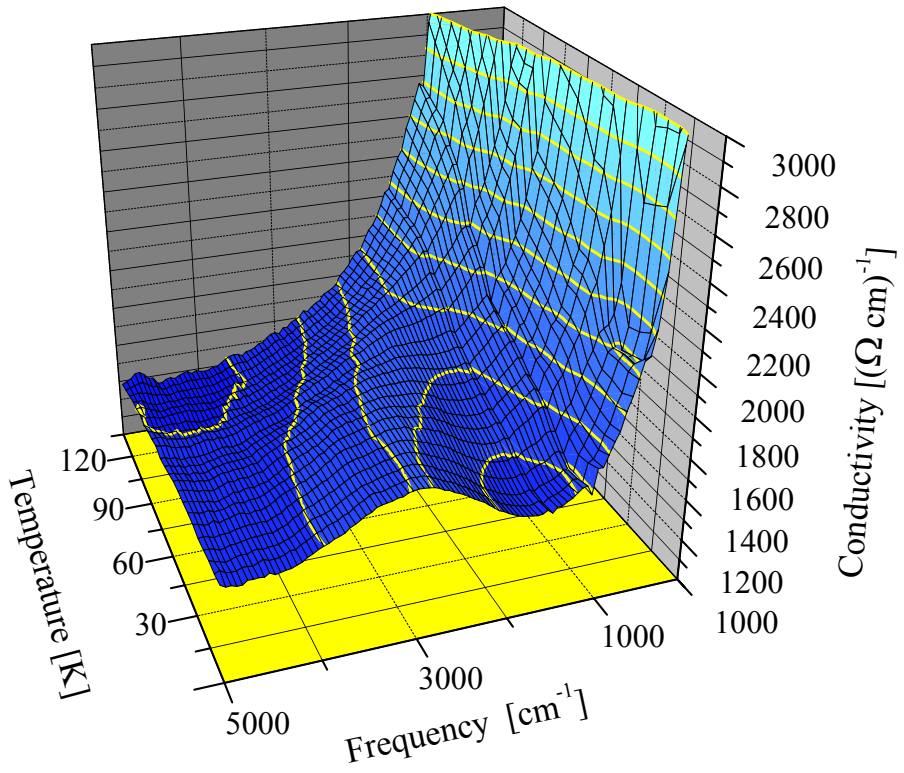

Figure 6.10: 3-d plot of the temperature-dependent optical conductivity of a holmium single crystal around the magnetic peak. The probing light was polarized parallel to the a-axis direction of the crystal.

vector of the radiation being either within the hcp basal planes (a-axis direction), or parallel to the c-axis direction. At higher temperatures, the flank of the Drude free-electron contribution is still visible. But with decreasing temperature, it swiftly rushes out of sight towards lower frequencies. The transition is much more pronounced for the measurement with c-axis polarized light, as it was already observed for the rare earths gadolinium, terbium and dysprosium.

It is not trivial, to extract the contribution of the magnetic peak out of the data. As described in the previous sections, the optical conductivity consists of several contributions, due to free electrons and transitions between

bands, all being temperature dependent. Thus, to gain information about the magnetic peak only, a detailed model, including all contributions, is necessary. The Drude-Lorentz model serves well on that purpose.

To illuminate the temperature dependence of the magnetic peak, further reflectivity spectra were taken between 5 K and 140 K at different temperatures. The measurements were carried out in the mid-infrared spectral region from 700 cm^{-1} to 7000 cm^{-1}. For extrapolation to lower and higher frequencies, necessary for the Kramers-Kronig transformation, the previously presented data (in coarse temperature steps) were used. This procedure was well applicable, as the extrapolated high- and low-frequency ranges show only minute changes with temperature, compared to the changes in the mid-infrared region. The resulting conductivity, in dependence of temperature, is plotted in the 3-d graphs of figure 6.9 and figure 6.10 in the vicinity of the magnetic peak. At the lowest measured temperatures (below 30 K), the peak is most pronounced and its position can be determined with the best precision. For c-axis polarized light, its maximum is located at 3170 cm^{-1}, and for a-axis polarized light it is slightly higher at 3300 cm^{-1}. This refers to an energy splitting of 0.39 eV and 0.41 eV respectively. In the publication of Krizek and Taylor [29], the exchange splitting for holmium was estimated to be 0.35 eV. Schüssler-Langeheine [63, 64] reports a splitting of about 0.52 eV for the Δ_2 band, which he examined by photoemission spectroscopy. The spectral weight of the transitions in the two directions of polarization differs for about 25%. this discrepancy is in accordance with the results of Knyazev and Sandratskii [28].

Figure 6.11 shows the fits of the magnetic feature at different temperatures, according to the Drude-Lorentz model. The temperature dependence of the peak position is plotted in figure 6.12. Over the whole temperature range the energy splitting is larger for the excitation in a-axis polarization. From 5 K to 110 K there is a small but monotonic decrease of the splitting in both directions of polarization. Above 100 K the fitting of the spectra becomes more and more difficult, as the magnetic peak becomes very small,

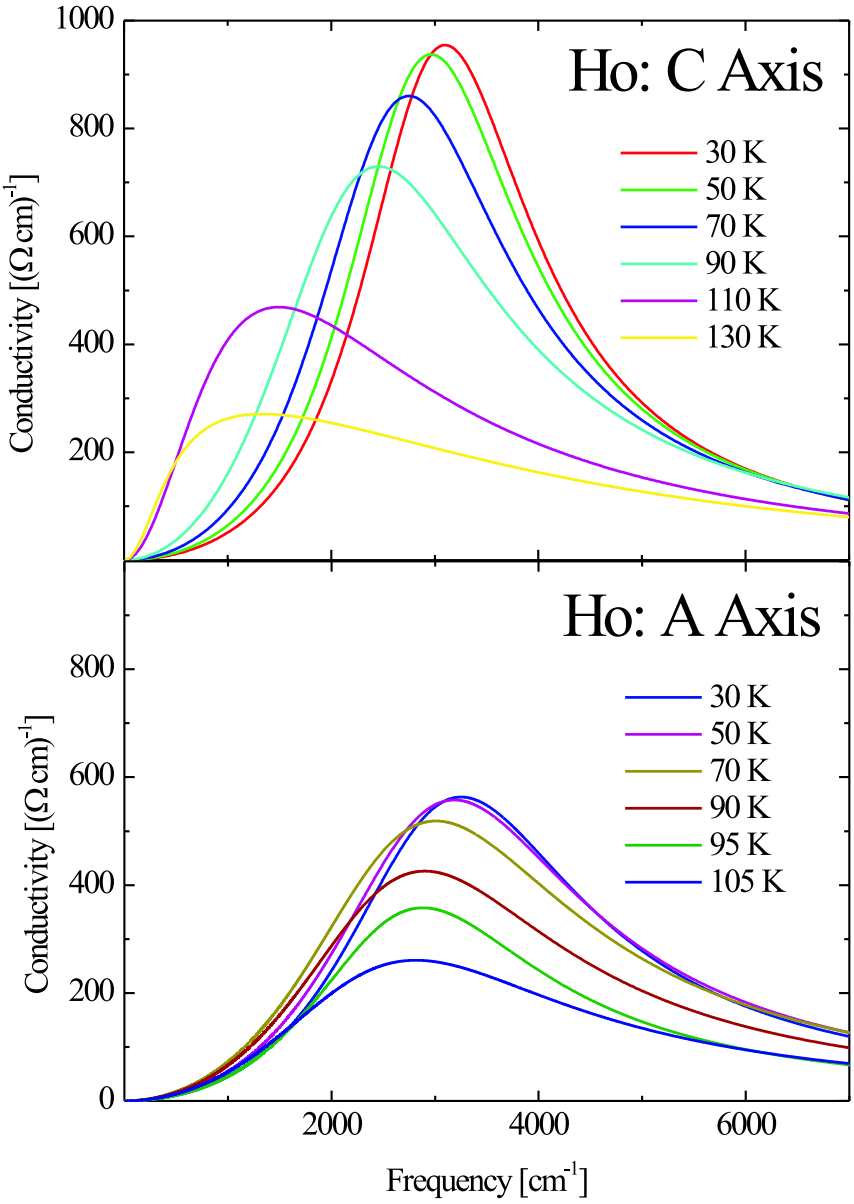

Figure 6.11: The measured reflectivity data were fitted according to the Drude-Lorentz model. Here are plotted the Lorentzian oscillators, that describe the magnetic peak in the model.

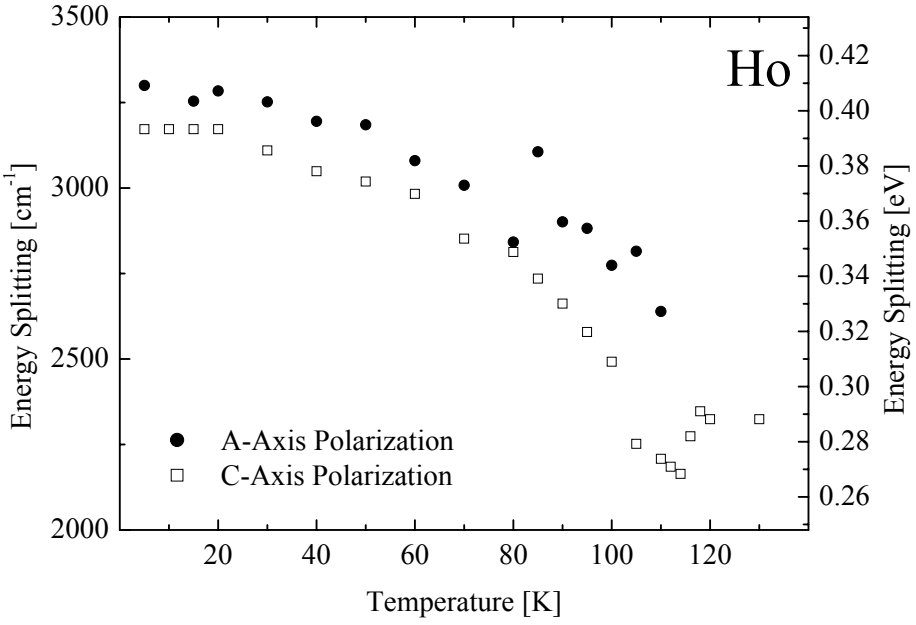

Figure 6.12: Plot of the temperature dependence of the magnetic band splitting in the two directions of polarization.

compared to the other contributions to the spectra (Drude free electrons, interband transitions). Above 110 K, the a-axis polarization peak is not to be detected anymore. The measured curve can be well fitted without any Lorentzian contribution in the mid-infrared range. On the other hand, for c-axis polarization, there is a contribution present even above Néel temperature. The measured reflectivity curve cannot be fitted properly, even above 133 K without assuming a Lorentzian oscillator in the region between 2000 cm^{-1} and 3000 cm^{-1}. Below 30 K, the magnetic feature shows no changes anymore. This confirms previous reports on other rare earth metals, that the magnetic splitting is not affected by the transition between antiferromagnetic and ferromagnetic state.

The photoemission measurements [63, 64], conducted on the collinearly ordered rare earth gadolinium clearly showed a strongly temperature depen-

dent, 'stoner-like' behaviour of the splitting energy, being proportional to the total magnetization of the bulk. This observation was explained by a rather delocalized electronic wave function within the respective band: The splitting then reflects the average orientation of the local 4f moments. In the same publication this 'stoner-like' behaviour was also reported for the antiferromagnetic phase of the rare earths, e.g. holmium. The explanation was supplied, that the probed band electrons are localized with respect to the c-axis direction, but delocalized within the hcp basal planes. Thus, the temperature dependent behaviour reflects the net magnetization within the ferromagnetic planes. On the other hand, the optical results of Knyazev and Sandratskii [28] for gadolinium, terbium and dysprosium show no temperature dependence in the energy splitting ('spin-mixing' behaviour), associating it with localized band electrons. This tendency is confirmed for holmium in this work. Nevertheless, the existence of an albeit small temperature dependence, as presented here, gives, in the context of the above argumentation, evidence of a sufficient degree of delocalization for the probed band, to let averaging effects become eminent.

6.2.5 Measurements with Magnetic Field

Of course, it was of particular interest, to examine the behaviour of the magnetic feature around 3000 cm^{-1} in an external magnetic field. The geometry of the measurements was according to figure 6.2. A magnetic field was applied along a-axis direction of the crystal, and the direction of light polarization was parallel to its c axis. Spectra were taken at zero field, at 1 T and 1.5 T, approaching from low field, again at 1 T and zero field, approaching from high field, and finally once more at 1 T, approaching from low field. Results for holmium in its antiferromagnetic phase are presented in figure 6.13. At 30 K the disturbing influence of thermal motion on the alignment of the magnetic moments is small. With no magnetic field applied, the magnetic feature shows up, according to the previous measurements. At a field of 1 T, the feature is reduced, and it finally vanishes at 1.5 T. According to

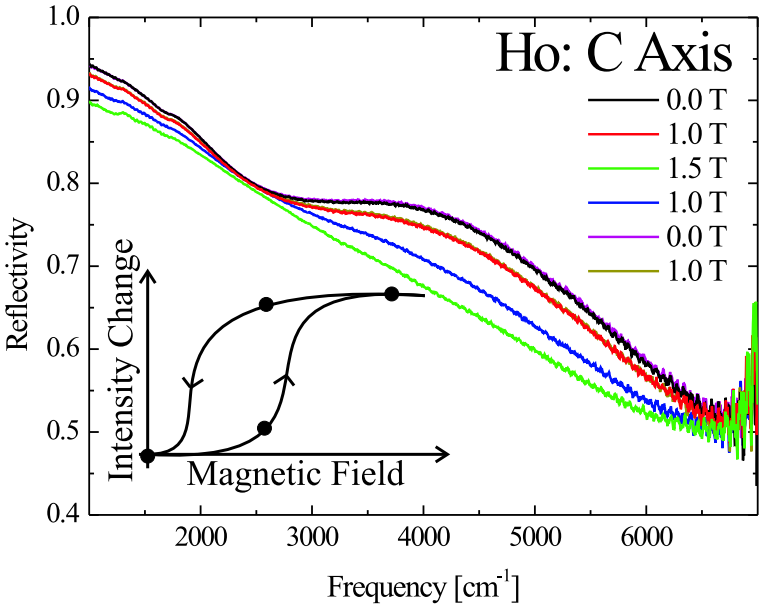

Figure 6.13: Change of the mid-infrared reflectivity spectrum of holmium on application of a magnetic field at 30 K in the antiferromagnetic phase. The magnetic field direction was along a axis and the polarization of the light parallel to c axis of the single crystal. The inset illustrates, how the measurement implies a hysteresis of the magnetic band splitting.

the measurements of Strandburg et a. [54] (see figure 3.4), at a field of 1.5 T, holmium has undergone an induced phase transition into a ferromagnetic state. An all-parallel orientation along the easy axis is imposed on the local magnetic moments.

The emergence of the magnetic feature in rare earth metals is generally explained by the splitting of valence-electron bands due to exchange interaction with the ordered local moments. But in the antiferromagnetic helical phase of holmium, one would expect the splitting to vanish, as the average moment over many crystal planes cancels out. This contradiction is solved

by the statement, that the respective band electrons are delocalized within the hcp basal planes but localized in the perpendicular c-axis direction. In this case, each electron only experiences the parallel order within each plane [67, 68, 63, 64].

Now, the following question arises: Why does the exchange splitting vanish, when not only within each basal plane, but even all over the whole crystal the local moments are aligned in a ferromagnetic manner? One would rather expect, that the splitting occurs more than ever: For the heavy rare earth elements, which show a linear ferromagnetic ordering (gadolinium, terbium and dysprosiom), the magnetic feature was reported [29, 28, 63, 64]. An explanation of the seeming contradiction might be a severe deformation of the Fermi surface due to the applied magnetic field, altering the spectrum of optical excitations, or even the exchange interaction itself. Or the spin-orbit coupling might be somehow weakened: In this case, the splitting would remain, but the transition could not be excited optically anymore. But there is one striking observation, that somehow softens those arguments: As sketched in the inset of figure 6.13, the removal and reapearance of the magnetic feature with altering field shows a hysteretic behaviour. After reducing the field from 1.5 T to 1 T, the feature does not regain its previous shape at 1 T. Only on reduction of the field back to zero, the original spectrum is reproduced. A hysteretic behaviour is not expected for (paramagnetic) band electrons, interacting directly with the external field, as they do not form magnetic domains. It rather implies an interaction of the band electrons with the (ordered) local moments, which, in turn, are influenced by the external field.

6.3 Measurements on Holmium Films

Metallic films, when compared to the bulk material, have several advantages with respect to infrared spectroscopy. For thin enough films, transmission measurements can be carried out. Thus, phase and intensity can be measured at the same time, making Kramers-Kronig analysis obsolete. Furthermore,

no reference mirror is needed. This extends the accessible frequency range to lower energies (as in reflection, sample reflectivity approaches reference reflectivity). But also for thick films, the sample preparation via evaporation holds some benefits. The problem of bulk single crystals, apart from its fabrication, is the proper surface preparation for optical measurements. The surface roughness needs to be small enough, to prevent scattering from taking influence on the spectra. But polishing and sawing might considerably disturb the single crystalline order beneath the surface. Evaporation under UHV-conditions yields perfectly flat, optical surfaces.

In this section, reflection measurements are presented, which were carried out on polycrystalline, 110 nm thick holmium films. The films were prepared and characterized, as described in chapter 5. The bottom line is, that infrared spectroscopy yields reproduceable results on evaporated holmium films. The characteristic features of the single crystal are reproduced, i.e. the purity of the films is sufficient, not to disturb the magnetic ordering within the material. The brief exposure to air, after the evaporation process, causes only thin oxide (hydroxide) layers, too thin to hamper the optical results. The effects of the silicon substrate can be properly taken into account for the Drude-Lorentz model, to refine the pure optical parameters of the holmium film. Furthermore, the behaviour of the mid-infrared magnetic feature is confirmed, according to the bulk measurements.

6.3.1 Holmium/Silicon: The Two-Layer System

Already at thicknesses around 100 nm, a considerable fraction of infrared light is transmitted even through a metallic film. The skin depth denotes the the thickness, after which the amplitude of the incident light is reduced by a factor of 1/e. This length is sketched in figure 6.14 for a polycrystalline holmium film at a temperature of 140 K. It is obvious from the graph, that an optical model, also in reflection geometry, has to take into account the substrate. The Kramers-Kronig analysis can no longer be performed, as the measured reflectivity is an intermixture of several different materials.

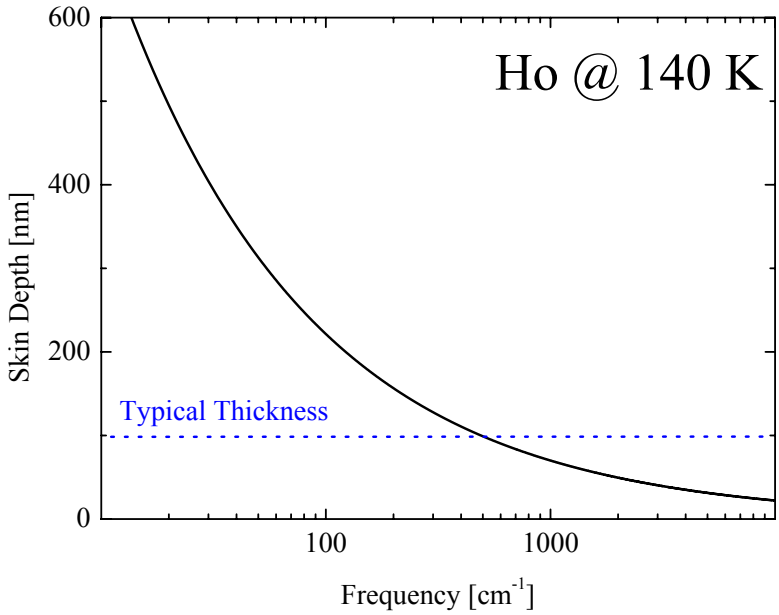

Figure 6.14: Plot of the calculated skin depth of infrared light in polycrystalline holmium at a temperature of 140 K, corresponding to a resistivity of 58 $\mu\Omega$ cm.

Still, the data can be fitted with the Drude-Lorentz model, but a multi-layer system has to be used. Each layer is fitted by a separate set of Drude-Lorentz parameters and the effective reflectivity is calculated for the total system (according to the thickness of each layer; see [5]). The parameters of the holmium film contribution then can be used for Kramers-Kronig analysis, to determine the frequency-dependent conductivity of the holmium-only film. For the modelling of the 400 μm thick silicon substrate, a simple scheme was used with one Lorentzian oscillator at the energy of the band gap (1.1 eV).

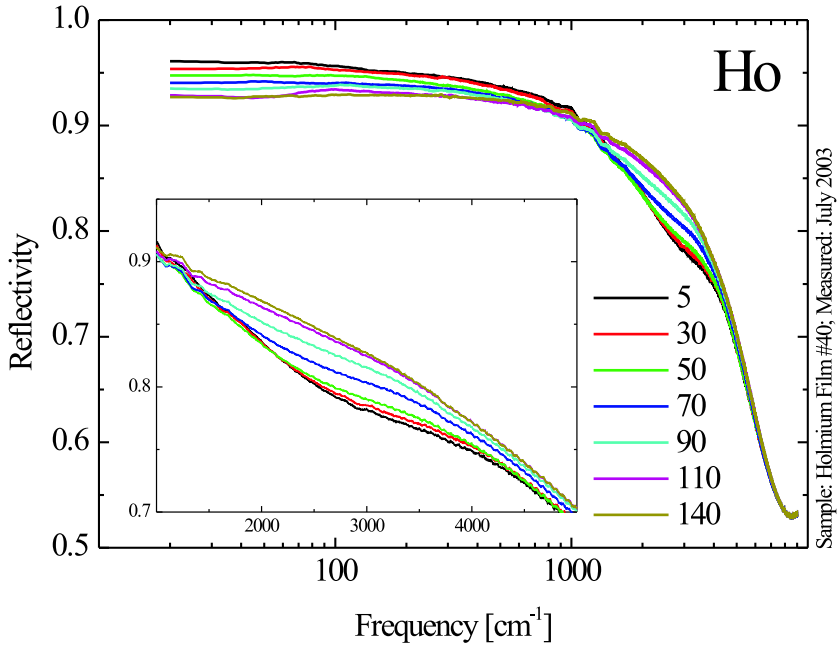

Figure 6.15: Reflectivity of the holmium film number 40 at different temperatures. The magnetic feature in the mid-infrared spectral range resembles that of the bulk crystal. At low frequencies, the reflectivity is reduced, due to transmission. This makes measurements possible down to lower frequencies.

6.3.2 Spectra of Holmium/Silicon

Reflectivity measurements were carried out on a 110 nm thick holmium film, evaporated on silicon substrate of 400 μm thickness. The (110) surface of the substrate was prepared, as described in section 5.1. Evaporation was performed at a working pressure of $1 \cdot 10^{-8}$ mbar on a room temperature substrate. The sample, denoted as film number 40, was annealed at a temperature of 120 °C for 16 h. Another sample was prepared for reflectivity measurements, to compare the absolute results for different films. This sample (denoted as film number 41) was evaporated at a pressure of $2 \cdot 10^{-9}$ mbar.

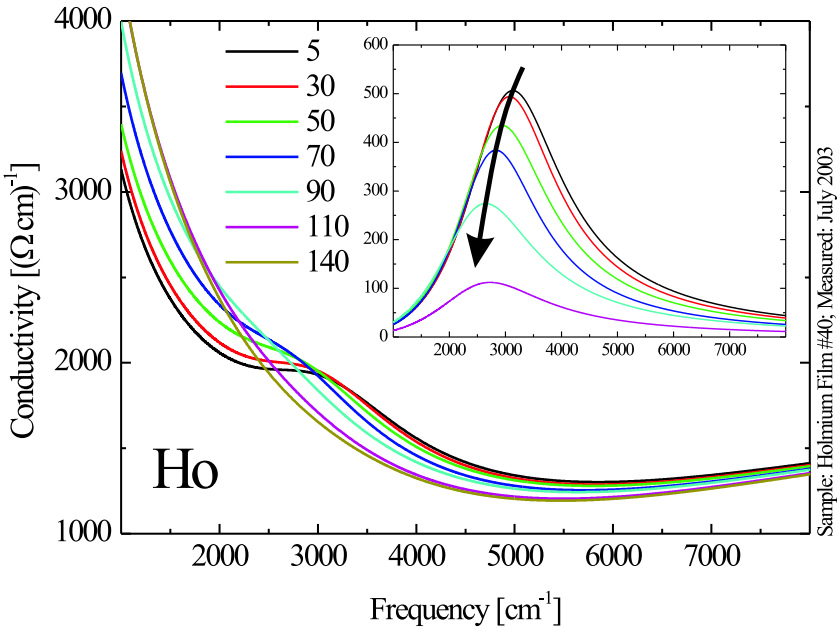

Figure 6.16: Conductivity of holmium film number 40 as result of a Drude-Lorentz fit to the measured reflectivity data. The conductivity contribution of the magnetic feature to the fit is depicted in the inset.

The other parameters were kept according to film number 40.

Figure 6.15 shows results of the reflectivity measurements on film number 40. Due to the partial transmission through the film, reflectivity in the far-infrared spectral region is remarkably reduced. The increased difference between reflectivity of sample and reference allows measurements down to 20 cm^{-1}. For the bulk measurements, it became problematic already at 50 cm^{-1}. The inset of figure 6.15 indicates, that for the film sample, the magnetic feature around 3000 cm^{-1} shows up, as it does for the bulk material. It is suppressed neither by the polycrystalline character of the film, nor by impurities. The characteristic magnetic properties are conserved. A detailed

analysis with the Drude-Lorentz model, as described in the previous section (6.3.1), yields the conductivity spectra, displayed in figure 6.16. The inset shows the contribution of the magnetic oscillator to the fit. The temperature dependence is confirmed, in accordance with the previously presented bulk measurements. Below 30 K, the magnetic peak saturates, with a centre frequency of about 3100 cm^{-1}. Above 110 K the contribution of the magnetic feature to the total spectrum becomes too small, to make a reasonable fit. The absolute magnitude of the peak is comparable to that of the single crystal in a-axis polarization. This qualitative finding is in accordance with the results, described in section 5.5: The film structure is polycrystalline with a preferred orientation of the crystallites' c-axis direction perpendicular to the substrate surface. In this case, the E-vector of the incident light probes more crystallites according to the a-axis polarization in the single-crystal measurements, giving a heavier weight to the respective spectrum.

The good reproducibility of the results is illustrated in figure 6.17. Reflectivity spectra of film number 40 an film number 41 are displayed. They coincide perfectly in the paramagnetic phase (140 K). In the magnetic phase, with increasing ordering of the magnetic moments, a slight deviation can be observed. Film number 41 was evaporated at a considerably better pressure ($2 \cdot 10^{-9}$ mbar) than film number 40 ($1 \cdot 10^{-8}$ mbar). Thus, the magnetic coupling in the latter film is slightly reduced due to impurities, and the former one shows the magnetic feature in a more pronounced manner.

The perfect coincidence in the paramagnetic phase leads to an important result: The films were fabricated under UHV conditions. But it was not possible, to conduct in-situ optical measurements. Thus, the samples had to be removed from the UHV chamber, and mounted in the spectrometer (there being under helium gas atmosphere). The exposure to air during transfer might give reason to worries, as the rare earth metals are well known for their reactivity. But still, holmium is much less reactive, than its colleges from the light part of the period (like cerium or europium). And experiments were reported [21, 10], which attested only a thin oxide layer formation on top

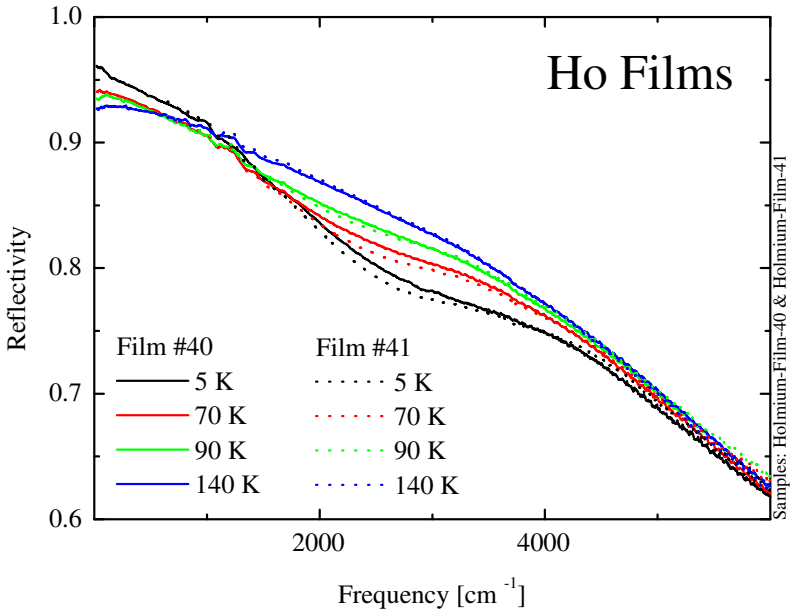

Figure 6.17: Comparison of the measured reflectivity of two different films. The behaviour of the two films is well reproducible. Only the magnitude of the magnetic feature is slightly different.

of rare earth films (in the order of some nanometres). The time of exposure to air of the two samples differed for hours, but nevertheless, the measured spectra are the same. The exposure of UHV-fabricated holmium films to air does not hamper infrared optical measurements!

The results of the infrared measurements on holmium films can be summarized in three points: First, it is possible, to model the two-layer system holmium/silicon properly with the Drude-Lorentz scheme, and to extract the pure properties of the holmium film from the measurements. Second, the holmium films reproduce the properties of the bulk material very well, when prepared in the described way. Third, it is possible, to fabricate holmium films with reproducible optical spectra. This shows, on the one hand, that the

fabrication process is relatively insusceptible to small changes of the fabrication parameters. On the other hand these results confirm, that the formation of any tarnish on top of the films ranges around thicknesses, which are well negligible for infrared optical measurements. This good-natured behaviour with respect to reproducibility, together with the ideal optical surfaces, makes these films the medium of choice for further exploration of rare earth metals towards lowest frequencies.

Chapter 7

Summary of the Results

In this work, optical properties of the rare earth metal holmium were explored in the infrared spectral region. Due to their localized magnetic moments, their oscillating, indirect exchange interaction, and their highly anisotropic Fermi surface, the rare earth metals feature a wide variety of magnetic ordering schemes, homlium being by far the most prosperous one [49, 51]. In the range from 50 cm^{-1} (6 meV) to 10000 cm^{-1} (1 eV), the temperature dependence of the spectra, and thus the dependance on the magnetic state, was explored for the transition from paramagnetic to antiferromagnetic and to ferromagnetic ordering. The spectroscopic technique was Fourier transform infrared spectroscopy (FTIR), and the measured quantity was reflectivity of the samples. By means of the Drude-Lorentz model, the reflectivity data were extrapolated, to yield, via Kramers-Kronig analysis, the frequency dependent conductivity. The Drude-Lorenz model allowed to separate different electronic contributions to the spectra, i.e. the Drude free-electron contribution and different excitations between localized states.

In the mid-infrared region, a temperature-dependent excitation was observed, which can be contributed to the energy splitting of electronic bands in the exchange field of the aligned local magnetic moments. The feature occurs below the Néel temperature of 133 K, saturates around 30 K, and shows no detectable changes anymore on transition to the ferromagnetic phase below

20 K. For holmium single crystals the optical measurements were carried out in two directions of polarization: Parallel and perpendicular to the hexagonal-close-packed (hcp) basal planes. These measurements confirmed the qualitative statement [28], that the magnetic peak is much more pronounced for light, which is polarized in c-axis direction of the crystal. The difference of the spectral weights in the saturation regime, measured with perpendicular polarizations, was determined to be 25 %. In contrast to earlier optical measurements, the sophisticated modelling revealed a temperature dependence of the splitting energy. At low temperatures, the peak of the transition centres at 3300 cm^{-1} (0.41 eV) and 3170 cm^{-1} (0.39 eV), for a-axis and c-axis polarization respectively. With increasing temperature, it shifts to lower frequencies. This observation can be brought into accordance with theoretical results [67, 68], which predict a different temperature-dependent behaviour for the exchange splitting, depending on the degree of localization in the respective band. It was suggested, that the valence bands might be more or less delocalized within the hcp basal planes but localized with respect to the c-axis direction of the crystal [63, 64]. In principle, the presented measurements confirm this description. But the temperature dependence in the optically probed data is much less pronounced, than the photoemission results [63, 64]. Thus, the optically probed part of the band structure is far more localized, in accordance to the considerations of Knyazev and Sandratskii[28]. For a-axis polarized light, the transition clearly vanishes, when approaching Néel temperature. But for c-axis polarization, a small contribution seems to remain, even in the paramagnetic phase, indicating a local interaction with the magnetic moments.

Furthermore, magnetic-field dependent measurements were carried out on holmium single crystals. It turned out, that, in the antiferromagnetic state, the magnetic peak in the spectra vanishes with increasing field. The change of the feature with field showed a hysteretic behaviour. The central question about this findings is: Why does the exchange splitting vanish, although the field imposes an ideal parallel ordering on the local magnetic

moments? Attempts of an explanation might be, that generally the Fermi surface becomes severely deformed in the external field, and thus, the optical excitation might not be possible anymore. The deformation of the Fermi surface might also directly change the exchange interaction between local moments and valence electrons. Or the spin-orbit coupling might be strongly reduced. Then the splitting might be still existent, but the transition is not an optically allowed one anymore. But both arguments are weak in one point: For an interaction of paramagnetic band electrons with an external field, one would not expect a hysteretic behaviour. In fact, the hysteresis rather implies an interaction of band electrons with the localized magnetic moments, which, in turn, are influenced by the external magnetic field. Further studies at different temperatures and fields might be required, to clarify the issue.

In the far-infrared spectral region measurements on bulk samples were carried out down to 50 cm^{-1}. The transport properties in this range are dominated by the Drude free-electron contribution. The measured dc resistivity was consistent with the low-frequency part of the spectra. But additionally, some extraordinary low-energy excitations were observed below 400 cm^{-1}. They are in accord with theoretical calculations [72], which predict an increased density of states in close vicinity of the Fermi niveau. This change in state density is the result of a hybridization of localized 4-f levels with outer valence-band states [69]. Measurements on evaporated films can help, to gain more detailed information on these low energy excitations.

Optical measurements on films give certain advantages over bulk measurements. Thus, holmium films were prepared under ultra-high vacuum (UHV) conditions, to avoid the problems of surface preparation, and to extend the range of measurements to even lower frequencies. With respect to the optical measurements, silicon substrate was regarded as the most suitable. Due to the high skin depth of the infrared radiation into metals, for reflectivity as well as transmittivity measurements, relatively thick films between 50 nm and 100 nm are reasonable. Film characterization was carried out by x-ray diffraction, SQUID, and resistivity measurements. The results showed, that

evaporation on a cold (room temperature) substrate, and subsequent long-term annealing at low temperatures (>10 h; <200 C), yields films with a relatively large grain size (about 60 nm), and a favourable orientation with their hcp basal planes within the film's plane. An oxide layer on top of the films was estimated to be only around 2 nm thick, even after long exposure to air. Optical spectra of the films reproduced the magnetic features of the bulk material in the expected degree. The reproducibility of measurements on different film samples confirmed, that the formation of a tarnish layer on top of the films presents no problem. It is thin, compared to the skin depth of infrared radiation into the metallic film. Last, but not least, it was shown, that the bilayer system of holmium and silicon can be well modelled by the Drude-Lorenz scheme, to extract the pure-holmium spectra from the measured bilayer data.

The infrared optical properties of bulk holmium were explored temperature- and magnetic-field dependent. Techniques for preparation, optical measurement, and evaluation of the data for holmium films were developed. Future effort can be put into transmission measurements on holmium films, to further push the frontier to lower frequencies. With the existing optical techniques it is then possible measure spectra down to 1 cm^{-1} (0.1 meV). The results will yield a deeper understanding of the behaviour of free electrons in the elementary local-moment systems, as well as allow a more detailed discussion of the observed low-frequency features. Additional experiments should also be carried out with respect to the magnetic-field dependence of the exchange splitting. Further measurements at different temperatures and at higher fields might help, to solve the open questions.

Scientific Constants

Constant	Symbol	Magnitude (MKS)	Unit (MKS)
Avogadro Constant	N_A	6.022136710^{23}	- mol^{-1}
Bohr Magneton	μ_B	9.274015410^{-24}	Am^2
Boltzmann Constant	k_B	$1.3806581 0^{-23}$	$J \cdot K^{-1}$
Electron Mass	m_e	9.109389710^{-31}	kg
Elementary Charge	e	$1.602177331 0^{-19}$	C
Gyromagnetic Constant	g_s	2.00232	-
Pi	π	3.141592654	-
Planck Constant	h	$6.62607551 0^{-34}$	J s
Planck Constant	$\hbar = \frac{h}{2\pi}$	$1.05457271 0^{-34}$	J s
Rydberg Constant	R_∞	$1.09737315341 0^{7}$	m^{-1}

These values are taken from [41, 45]

Bibliography

[1] M. N. Baibich, J. M. Broto, A. Fert, F. Nguyen Van Dau, F. Petroff, P. Eitenne, G. Creuzet, A. Friederich, J. Chazelas, *Phys. Rev. Lett.*, **61**, 2472 (1988).

[2] G. Binasch, P. Grünberg, F. Sauerbach, W. Zinn, *Phys. Rev. B*, **39**, 4828 (1989).

[3] D. Bürgler, P. Grünberg, *Magnetoelectronics: Exchange Anisotropy, Interlayer Exchange Coupling, GMR, TMR, and Current-Induced Magnetic Swiching*, in *Neue Materialien für die Informationstechnologie, Vorlesungsskripte des 32. IFF-Ferienkurses*, Vol. VII, (Schriften des Forschungszentrums Jülich, Materie und Material/Matter and Materials, 2002).

[4] G. K. T. Conn, D. G. Avery, *Infrared Methods, Principles and Applications* (Academic Press, New York and London, 1960).

[5] M. Dressel and G. Grüner, *Electrodynamics of Solids* (Cambridge University Press, 2002).

[6] P. R. Griffiths, J. A. de Haseth, *Fourier Transform Infrared Spectrometry* (John Wiley and Sons, New York, Chichester, Brisbane, Toronto, Singapore, 1986).

[7] M. F. Kimmitt, *Far-Infrared Techniques* (Pion Limited, London, 1970).

[8] P. W. Kruse, L. D. McGlauchlin, R. B. McQuistan, *Elements of Infrared Technology: Generation, Transmission, and Detection* (John Wiley and Sons, Inc., New York, London, 1962).

[9] K. D. Möller, W. G. Rothschild, *Far-Infrared Spectroscopy* (Wiley-Interscience, New York, London, Sydney, Toronto, 1971).

[10] A. K. Burnham, G. T. Jameson, *J. Vac. Sci. Technol. A 5*, **4**, 1713 (1987).

[11] H. T. G. Hentzell, C. R. M. Grovenor, D. A. Smith, *J. Vac. Sci. Technol. A 2*, **2**, 218 (1984).

[12] D. A. Jehan, D. F. McMorrow, R. A. Cowley, R. C. C. Ward, M. R. Wells, N. Hagman, K. N. Clausen, *Phys. Rev. B*, **48**, 5594 (1993).

[13] G. Kaindl, A. Hhr, E. Weschke, S. Vandré, C. Schüßler-Langeheine, C. Laubschat, *Phys. Rev. B*, **51**, 7920 (1995).

[14] J. Kwo, E. M. Gyorgy, D. B. McWhan, M. Hong, F. J. DiSalvo, J. E. Bower, *Phys. Rev. Lett.*, **55**, 1402 (1985).

[15] T. Marcinow, K. Truszkowska, *Appl. Opt.*, **20**, 1755 (1981).

[16] G. A. Mulhollan, K. Garrison, J. L. Erskine, *Phys. Rev. Lett.*, **69**, 3240 (1992).

[17] M. Ohring, *The Materials Science of Thin Films* (Academic Press, Inc., Boston, San Diego, New York, London, Sydney, Tokyo, Toronto, 1992).

[18] R. D. Thompson, B. Y. Tsaur, K. N. Tu, *Appl. Phys. Lett.*, **38**, 535 (1981).

[19] T. Trappmann, M. Gajdzig, C. Sürgers, H. v. Löhneysen, *Europhys. Lett.*, **39**, 159 (1997).

[20] S. Vandré, T. Kalka, C. Preinesberger, M. Dähne-Prietsch, *Phys. Rev. Lett.*, **82**, 1927 (1999).

[21] D. Weller, D. D. Sarma, *Surf. Sci.*, **171**, L425 (1986).

[22] B. Cullity, *Elements of X-Ray Diffraction*,(Addison Wesley, Reading, MA, 1978).

[23] M. Münch, *Strukturelle Beeinflussung der elektrischen Transporteigenschaften dnner organischer Schichten*,(PhD. Thesis at the Department of Physics, University of Stuttgart, 2001).

[24] D. W. Lynch and W. R. Hunter, *Comments on the Optical Constants of Metals and an Introduction to the Data for Several Metals* in *Handbook of Optical Constants of Solids* , VolI, edited by E. D. Palik (Accademic Press, San Diego, London, Boston, New York, Sydney, Tokyo, Toronto, 1998), p. 275.

[25] D. E. Aspines, *The Accurate Determination of Optical Properties by Ellipsometry* in *Handbook of Optical Constants of Solids* , VolI, edited by E. D. Palik (Accademic Press, San Diego, London, Boston, New York, Sydney, Tokyo, Toronto, 1998), p. 89.

[26] D, Y. Smith, *Dispersion Theory, Sum Rules, and Their Application to the Analysis of Optical Data* in *Handbook of Optical Constants of Solids* , Vol.I, edited by E. D. Palik (Accademic Press, San Diego, London, Boston, New York, Sydney, Tokyo, Toronto, 1998), p. 35.

[27] J. G. Endriz, W. E. Spicer, *Phys. Rev. B*, **2**, 1466 (1970).

[28] Y. V. Knyazev, L. M. Sandratskii, *J. Phys.: Condens. Matter*, **3**, 9667 (1991).

[29] J. Krizek and K. N. R. Taylor, *J. Phys. F: Metal Phys.*, **5**, 774 (1975).

[30] S. H. Liu, *Electronic Structure of Rare Earth Metals* in *Handbook on the Physics and Chemistry of Rare Earths* , Vol.I, edited by K. A. Gschneider, L. R . Eyring, (North-Holland Publishing Company, Amsterdam, New York, Oxford, 1978), p. 233.

[31] H. P. Myers, *J. Phys. F: Metal Phys.*, **6**, 141 (1976).

[32] J. H. Weaver and D. W. Lynch, *Phys. Rev. Lett.*, **34**, 1324 (1975).

[33] P. Drude, *Ann. Physik*, **1**, 566 (1900) and **3**, 369 (1900).

[34] P. Drude, *Phys. Z.*, **1**, 161 (1900).

[35] U. Mizutani, *Electron Theory of Metals*, (Cambridge University Press, 2001).

[36] S. Legvold, *Transport Properties*, in *Magnetic Properties of Rare Earth Metals* , edited by R. J. Elliott (Plenum Press, London and New York, 1972).

[37] J. M. Fournier, E. Gratz, *Transport Properties of Rare Earth and Actinide Intermetallics*, in *Handbook of the Physics and Chemistry of Rare Earths* , Vol.XVII, edited by K. A. Gschneider, Jr., L. Eyring, G. H. Lander and G. R. Choppin (North-Holland, Amsterdam, London, New York, Tokyo, 1993).

[38] W. Nolting, *Grundkurs Theoretische Physik: Elektrodynamik*, (Zimmermann-Neufang, Ulmen, 1993).

[39] L. D. Landau, E. M. Lifschitz, *Quantum mechanics : non-relativistic theory* in *Course of theoretical physics*, Vol. III, (Oxford , Frankfurt : Pergamon Pr., 1965).

[40] J. C. Slater, *Quantum Theory of Matter*, (Mc Graw-Hill Book Company, New York, St. Louis, San Francisco, Toronto, London, Sydney, 1968).

[41] P. A. Tipler, *Physics for Scientists and Engineers*, (W. H. Freeman Co, 1999).

[42] H. Haken, H, C. Wolf, *Atomic and Quantum Physics*, (Heidelberg: Springer, 1987).

[43] S. V. Vonsovskii, *Magnetism*, Vol. I, (John Wiley & Sons, New York, Toronto, 1971).

[44] N. W. Ashcroft, N. D. Mermin, *Solid State Physics*, (Saunders College Publishing, Harcourt Brace College Publishers, Fort Worth, Philadelphia, San Diego, New York, Orlando, Austin, San Antonio, Toronto, Montreal, London, Sydney, Tokyo, 1976).

[45] Ch. Kittel, *Introduction to Solid State Physics*, (New York: Wiley, 1986).

[46] R. J. Elliott, *Magnetic Properties of Rare Earth Metals*, (Plenum Press, London and New York, 1972).

[47] A. J. Freeman, *Energy Band Structure, Indirect Exchange Interactions and Magnetic Ordering*, in *Magnetic Properties of Rare Earth Metals* , edited by R. J. Elliott (Plenum Press, London and New York, 1972).

[48] J. J. Rhyne, *Bulk Magnetic Properties*, in *Magnetic Properties of Rare Earth Metals* , edited by R. J. Elliott (Plenum Press, London and New York, 1972).

[49] J. Jensen, A. R. MacKintosh, *Rare Earth Magnetism*, (Clarendon Press, Oxford, 1991).

[50] W. C. Koehler, J. W. Cable, M. K. Wilkinson, and E. O. Wollan, *Phys. Rev.*, **151**, 414 (1966).

[51] W. C. Koehler, *Magnetic Structures of Rare Earth Metals and Alloys*, in *Magnetic Properties of Rare Earth Metals* , edited by R. J. Elliott (Plenum Press, London and New York, 1972).

[52] S. H. Liu, *Phys. Rev.*, **121**, 451 (1961).

[53] E. Schreier, *Myon-Spin-Rotation und -Relaxation zur Untersuchung magnetischer Eigenschaften der Schweren Seltenen Erden*, **121**, 451

(Dissertation an der Fakultt Physik der technischen Universitt Mnchen, 1999).

[54] D. L. Strandburg, S. Legvold, and F. H. Spedding, *Phys. Rev.*, **127**, 2046 (1962).

[55] M. W. Stringfellow, T. M. Holden, B. M. Powell and A. D. B. Woods, *J. Phys. C: Metal Phys. Suppl.*, **2**, S189 (1970).

[56] K. Yosida, *Phys. Rev.*, **106**, 893 (1957).

[57] A. T. Hindmarch, B. J. Hickey, *Phys. Rev. Lett.*, **91**, 116601-1 (2003).

[58] A. H. Mitchel, *Phys. Rev.*, **105**, 1439 (1957).

[59] M. A. Ruderman, C. Kittel, *Phys. Rev.*, **96**, 99 (1954).

[60] R. E. Watson, A. J. Freeman, *Phys. Rev.*, **152**, 566 (1966).

[61] R. E. Watson, A. J. Freeman, *Phys. Rev.*, **178**, 725 (1969).

[62] B. Kim, A. B. Andrews, J. L. Erskine, K. J. Kim, B. N. Harmon, *Phys. Rev. Lett.*, **68**, 1931 (1992).

[63] C. Schüßler-Langeheine, *Magnetic Properties of Thin Films of Heavy Lanthanide Metals Studied by Magnetic X-Ray Diffraction and High-Resolution Photoemission*, (PhD. Thesis, Department of Physics, Freie Universitt Berlin, 1999).

[64] C. Schüßler-Langeheine, E. Weschke, H. Ott, A. Yu. Grigoriev, A. Möller, R. Meier, Chandan Mazumdar, G. Kaindl, *J. Electron Spectrosc.*, **114-116**, 795 (2001).

[65] C. Schüßler-Langeheine, R. Meier, H. Ott, Z. Hu, Chandran Mazumdar, A. Yu. Grigoriev, G. Kaindl, E. Weschke, *Phys. Rev. B*, **60**, 3449 (1999).

[66] G. A. Mulhollan, K. Garrison, J. L. Erskine, *Phys. Rev. Lett.*, **69**, 3240 (1992).

[67] W. Nolting, T. Dambeck, G. Borstel, *Z. Phys. B*, **94**, 409 (1994).

[68] W. Nolting, S. Rex, S. M. Jaya, *Correlation Effects in the Quasiparticle Bandstructure of Local Moment Systems*, in *Magnetism and Electronic Correlations in Local-Moment Systems: Rare Earth Elements and Compounds*, edited by M. Donath, P. A. Dowben, W. Nolting, (Worls Scientific, Singapore, New Jersey, London, Hong Kong, 1998).

[69] L. Petit, A. Savane, Z. Szotek, P. Strange, H. Winter, W. M. Temmerman, *J. Phys: Condens. Matter*, **13**, 8697 (2001).

[70] H. L. Skriver, I. Mertig, *Phys. Rev B*, **41**, 6553 (1990).

[71] S. A. Sondhelm, R. C. Young, *J. Phys. F: Met. Phys.*, **15**, L261 (1985).

[72] H. Winter, *Private Communication*, (2003).

[73] B. J. Beaudry, K. A. Gschneider, Jr., *Preparation and Basic Properties of the Rare Earth Metals*, in *Handbook of the Physics and Chemistry of Rare Earths* , Vol.I, edited by K. A. Gschneider, Jr., L. Eyring, (North-Holland Publishing Company, Amsterdam, New York, Oxford, 1978).

[74] W. Shakespeare, *Hamlet*, (1601/02).

Curiculum Vitae

April 17, 1973	Born in Neuss, Germany
08/79 - 07/83	Martin-Luther-Grundschuhle, Neuss
08/83 - 06/92	Quirinus-Gymnasium Neuss
06/92	Abitur (High School Graduation)
07/92 - 06/93	Military Service; Air Force, Budel/Kerpen
08/93 - 03/00	Studies of Physics at the Heinrich-Heine-Universität Düsseldorf
10/96 - 06/97	Studies of Physics at the University of Edinburgh
03/00	Diploma in Physics The thesis was conducted at the Institut für Lasermedizin, Heinrich-Heine-Universität Düsseldorf, under supervision of Prof. Dr. Peter Hering. The topic was: Development and Test of a Small-Bandwidth Continuously Tunable IR Laser System for High-Sensitive Trace-Gas Analysis
04/00 - Present	Research assistant at the 1. Physikalisches Institut, Universität Stuttgart, under supervision of Prof. Dr. Martin Dressel

Acknowledgements

First and foremost, I wish to thank Prof. Dr. Martin Dressel for giving me the opportunity, to work on this exciting project at his department. I gratefully acknowledge his continuous support and encouragement. Furthermore I want to thank Prof. Dr. Gisela Schütz for co-assessing this thesis.

I wish to especially thank Gabriele Untereiner and Dr. Bruno Gompf for the generous support in all questions, scientific as well as technical ones. My further thanks go to Tobby Brandt, for hours of fruitful discussions related to vacuum technology, and Philipp Haas, as well as Dr. Christine Kuntscher and Dr. Michael Dumm for the introduction to Fourier-Transform Spectrometry and plenty of helpful conversation.

Furthermore, I want to thank Dr. Hermann Winter (Forschungszentrum Karlsruhe) for conducting the DOS-calculations on holmium, and Stephan Hirschman (Kristalllabor, Uni Stuttgart) for the x-ray diffraction measurements. For helpful discussions on the topic of rare earth metals, my thanks go to Enrico Schierle, Dr. Christian Schüßler-Langeheine, and Dr. habil. Eugen Weschke(FU Berlin/ Universität zu Köln).

I also want to pay tribute to the support, I experienced from our department's machine shop. My thanks go to Rolf Heckhorn, Ralf Kamella, and all associates.

Special thanks I want to express towards Stephan Mair and Marc Scheffler for their support and friendship from the very beginning of my time in Stuttgart. Furthermore I wish to thank all colleagues for the pleasant atmosphere, culminating in the weekly attendance at O'Reillys pub quiz. I

thank all the friends, I met during my time in Düsseldorf, Edinburgh, and Stuttgart, as well as De Dolle, giving me the reassurance, that "There are more things in heaven and Earth..." [74].

Finally I want to thank my parents for everything and Juliane Meyer auf der Heyde for the continuous encouragement and much more.

Erklärung

Hiermit erkläre ich, dass die vorliegende Arbeit von mir eigenhändig verfasst wurde und keine anderen, als die angegebenen Quellen und Hilfsmittel verwandt wurden.

Stuttgart, den 29. April 2004